Human Molecular Genetics, 2016, Vol. 25, No. 24 5365–5382

doi: 10.1093/hmg/ddw352
Advance Access Publication Date: 29 October 2016
Original Article

ORIGINAL ARTICLE

Human R1441C LRRK2 regulates the synaptic vesicle proteome and phosphoproteome in a *Drosophila* model of Parkinson's disease

Md Shariful Islam[1,2,3,†], Hendrik Nolte[2,†], Wright Jacob[4], Anna B. Ziegler[5,6,7], Stefanie Pütz[8], Yael Grosjean[5,6,7], Karolina Szczepanowska[9], Aleksandra Trifunovic[2,9,10], Thomas Braun[11], Hermann Heumann[1], Rolf Heumann[4], Bernhard Hovemann[8], Darren J. Moore[3,*] and Marcus Krüger[2,10,11,*]

[1]Silantes GmbH, Munich, Germany, [2]Institute for Genetics, Cologne Excellence Cluster on Cellular Stress Responses in Aging-Associated Diseases (CECAD), Cologne, Germany, [3]Center for Neurodegenerative Science, Van Andel Research Institute, Grand Rapids, Michigan, USA, [4]Biochemistry II, Molecular Neurobiochemistry Faculty for Chemistry and Biochemistry Ruhr-University Bochum, NC 7/174 Universitaetsstraße 150, 44780 Bochum, Germany, [5]CNRS, UMR6265 Centre des Sciences du Goût et de l'Alimentation, F-21000 Dijon, France, [6]INRA, UMR1324 Centre des Sciences du Goût et de l'Alimentation, F-21000 Dijon, France, [7]Université de Bourgogne Franche-Comté, UMR Centre des Sciences du Goût et de l'Alimentation, F-21000 Dijon, France, [8]Faculty for Chemistry and Biochemistry, Ruhr-University Bochum, AG Molecular Cell Biochemistry, Universitaetsstraße 150, 44780 Bochum, Germany, [9]Institute for Mitochondrial Diseases and Aging, Medical Faculty, University of Cologne, D-50931 Cologne, Germany, [10]Center for Molecular Medicine (CMMC), University of Cologne, Germany and [11]Max Planck Institute for Heart and Lung Research, Ludwigstr. 43, 61231 Bad Nauheim, Germany

*To whom correspondence should be addressed at: Marcus Krüger, Institute for Genetics, Cologne Excellence Cluster on Cellular Stress Responses in Aging-Associated Diseases (CECAD), Cologne, Germany. E-mail: marcus.krueger@uni-koeln.de; Darren J. Moore, Center for Neurodegenerative Science, Van Andel Research Institute, Grand Rapids, Michigan, USA. E-mail: Darren.Moore@vai.org

Abstract

Mutations in *leucine-rich repeat kinase 2* (*LRRK2*) cause late-onset, autosomal dominant familial Parkinson's disease (PD) and variation at the *LRRK2* locus contributes to the risk for idiopathic PD. LRRK2 can function as a protein kinase and mutations lead to increased kinase activity. To elucidate the pathophysiological mechanism of the R1441C mutation in the GTPase domain of LRRK2, we expressed human wild-type or R1441C LRRK2 in dopaminergic neurons of *Drosophila* and observe reduced locomotor activity, impaired survival and an age-dependent degeneration of dopaminergic neurons thereby creating a new PD-like model. To explore the function of LRRK2 variants *in vivo*, we performed mass spectrometry and quantified 3,616 proteins in the fly brain. We identify several differentially-expressed cytoskeletal, mitochondrial and synaptic vesicle proteins (SV), including synaptotagmin-1, syntaxin-1A and Rab3, in the brain of this LRRK2 fly model. In addition, a global phosphoproteome analysis reveals the enhanced phosphorylation of several SV proteins, including synaptojanin-1 (pThr1131) and the

[†]These authors contributed equally to this work.
Received: September 13, 2016. **Revised:** October 6, 2016. **Accepted:** October 11, 2016

microtubule-associated protein futsch (pSer4106) in the brain of R1441C hLRRK2 flies. The direct phosphorylation of human synaptojanin-1 by R1441C hLRRK2 could further be confirmed by *in vitro* kinase assays. A protein–protein interaction screen in the fly brain confirms that LRRK2 robustly interacts with numerous SV proteins, including synaptojanin-1 and EndophilinA. Our proteomic, phosphoproteomic and interactome study in the *Drosophila* brain provides a systematic analyses of R1441C hLRRK2-induced pathobiological mechanisms in this model. We demonstrate for the first time that the R1441C mutation located within the LRRK2 GTPase domain induces the enhanced phosphorylation of SV proteins in the brain.

Introduction

Parkinson's disease (PD) is the most common neurodegenerative movement disorder affecting 1–2% of individuals over 60 years of age (1,2). PD is primarily characterized by the selective loss of dopaminergic neurons in the substantia nigra pars compacta and the appearance of α-synuclein-positive Lewy bodies in remaining neurons of the brainstem. PD is typically an idiopathic disease of unclear aetiology, however, in 5–10% of cases, PD is inherited and mutations in at least 12 genes have so far been unambiguously identified to cause familial PD. Mutations in the *leucine-rich repeat kinase 2* (*LRRK2*, *PARK8*) gene cause late-onset, autosomal dominant PD and represent the most common cause of familial PD (3–6). At least seven missense mutations (i.e. R1441C/G/H, N1437H, Y1699C, G2019S and I2020T) are considered to be pathogenic based upon the segregation of these variants with disease in families with PD (7). Further linking *LRRK2* to PD, common variation at the *LRRK2* genomic locus is associated with an increased risk of idiopathic PD (8). *LRRK2* encodes a 2527 amino-acid protein containing multiple domains, including leucine-rich repeats (LRR), a Ras-of-Complex (Roc) GTPase domain, a C-terminal-of-Roc (COR) domain, a tyrosine-kinase-like protein kinase domain and WD40 repeats, potentially suggesting myriad protein interactions and cellular functions (3–6). Accordingly, LRRK2 exhibits GTPase and kinase activity at least *in vitro*. Disease-causing mutations tend to cluster within the central Roc-COR tandem and kinase domains of LRRK2 where they can impair GTPase activity or enhance kinase activity, respectively. Therefore, alterations in GTPase and kinase activity most likely underlie the development of PD due to *LRRK2* mutations (9–11).

While much attention has so far focused on the kinase activity of LRRK2 (9–11), direct substrates of phosphorylation are poorly described in living organisms and it is not clear how kinase activity contributes to neurodegeneration induced by different *LRRK2* mutations. The most common G2019S mutation, located in the kinase activation loop, markedly enhances LRRK2 kinase activity and induces neuronal toxicity (12,13). A recent phosphoproteomic screen in mouse embryonic fibroblasts harbouring the G2019S mutation in LRRK2 identified the enhanced phosphorylation of a subset of Rab GTPases, including Rab10 and Rab12, potentially representing the first *bonafide* substrates of LRRK2 in cells or tissues (14). Importantly, familial mutations in LRRK2 commonly increase the phosphorylation of selected Rabs in mammalian cells, similar to the effects of familial mutations on LRRK2 autophosphorylation at Ser1292, indicating that familial PD mutations may share the capacity to enhance LRRK2 kinase activity given the proper substrate and/or cellular context. Prior studies have shown that the R1441C/G/H and Y1699C mutations in the Roc-COR tandem domain consistently impair GTPase activity and potentially elevate GTP binding capacity, which most likely mediates their effect on kinase activity (15–18). Consistent with these observations, GTP binding capacity via the Roc domain is critically required for normal kinase activity (19). At present, it is unclear which kinase substrates are directly targeted by familial LRRK2 variants and in which cellular context, especially in brain tissue. A brain-specific phosphoproteomic screen of LRRK2 harbouring a familial PD mutation would provide important insight into how LRRK2 kinase activity is associated with neurodegeneration and the underlying mechanisms involved. LRRK2 has so far been reported to directly phosphorylate a number of mammalian proteins *in vitro*, including moesin, β-tubulin, ArfGAP1, OPA1, RGS2, RPS15, Snapin, Rab5b and MARK1, but whether these phosphorylation events also occur *in vivo* remains unclear (20–28). In *Drosophila* models expressing G2019S LRRK2, the phosphorylation of a number of proteins, including 4E-BP1, FoxO1, Futsch and Endophilin A (EndoA), is increased in the brain. The synaptic vesicle forming protein EndoA is phosphorylated at Ser75 in a LRRK2-dependent manner which inhibits the membrane association of EndoA and disrupts EndoA-mediated synaptic vesicle endocytosis (29).

In the present study, we selected the fruitfly as a model system to investigate the pathogenic consequences of overexpressing human LRRK2 harbouring a R1441C mutation in dopaminergic neurons. Several studies have shown that human LRRK2 mutations can induce phenotypes in *Drosophila* that resemble the hallmarks of PD (30–32). Furthermore, LRRK2 overexpression in flies is reported to alter microtubule dynamics leading to dysfunctional synaptic morphology (33). Here, we used a stable isotope labelling (SILAC) approach in the fly to accurately quantify LRRK2-dependent alterations in proteins and phosphopeptides and identify LRRK2 interaction partners by high resolution mass spectrometry. The overexpression of human wild-type (WT) and R1441C LRRK2 using a Gal4/UAS system results in clear age-dependent PD-related phenotypes, including motor deficits, reduced survival and dopaminergic neuronal degeneration. In total, we identified 83, 226 and 340 proteins that are significantly regulated by R1441C LRRK2 overexpression compared to WT LRRK2 and control flies at days 1, 10 and 30, respectively. A particularly important function of LRRK2 is its kinase activity which is enhanced by familial mutations. To gain insight into LRRK2-dependent signalling pathways and direct phosphorylation targets, we performed a global phosphoproteome analysis of *Drosophila* brain and identified >6,000 phosphorylation sites on ~2,000 proteins. We identified a number protein phosphorylation sites that are regulated by human LRRK2 variants. Taken together, our *in vivo* quantitative SILAC proteomic approach has identified for the first time putative novel LRRK2 kinase substrates and signalling pathways in the *Drosophila* brain.

Results

Overexpression of human WT and R1441C LRRK2 in the *Drosophila* retina induces photoreceptor degeneration

The Gal4/UAS expression system has been widely used in *Drosophila* to ectopically express transgenes in a tissue-specific manner. To evaluate whether human LRRK2 (hLRRK2) and its PD-linked mutations have an impact on neuronal cell homeostasis in *Drosophila*, we first generated transgenic strains which overexpress WT or R1441C hLRRK2 under the control of the glass

multiple reporter (GMR) (34). Here, we used the degeneration of photoreceptor cells to determine whether WT or R1441C hLRRK2 overexpression induces neurodegeneration in flies. Both strains expressing hLRRK2 (WT or R1441C) are expressed at equivalent levels in the retina (Fig. 1A) . An optical neutralization technique was used to follow the kinetics of retinal degeneration over a time period of seven weeks. We measured at least 90 ommatidia (each containing 7 rhabdomeres) from six flies per genotype and detect a mild but progressive degeneration of photoreceptors overexpressing WT hLRRK2 compared to *Canton-S* control flies (Fig. 1B and C). The overexpression of R1441C hLRRK2 induces the severe and rapid degeneration of photoreceptors compared to WT hLRRK2 and control flies ($P < 0.05$) (Fig. 1B and C). Our data are consistent with previous reports demonstrating that WT or G2019S hLRRK2 expression induces retinal degeneration in *Drosophila* (32,33).

Reduced survival and motoric deficits in WT and R1441C hLRRK2 *Drosophila* strains

Next, we elected to explore LRRK2-induced pathobiology in dopaminergic neurons. We overexpressed WT and R1441C hLRRK2 specifically in the dopaminergic neurons by combining UAS-hLRRK2 transgenic strains with a *ddc-gal4* driver strain (35). Since both hLRRK2 variants are fused with an N-terminal FLAG-tag, Western blot analysis of fly head extracts with an anti-FLAG antiserum reveals similar expression levels of WT and R1441C hLRRK2 in brain tissue (Fig. 1D). To further investigate the phenotype of flies expressing hLRRK2 variants, we measured the survival of control (*ddc-gal4* and UAS-hLRRK2), WT hLRRK2 and R1441C hLRRK2 flies. Our data demonstrate that WT hLRRK2 flies exhibit a significantly shorter median life span (−17%) compared to control flies, whereas R1441C hLRRK2 transgenic flies show an even larger reduction of the median life span (−34%) (Fig. 1E). Our data indicate that hLRRK2 expression selectively in dopaminergic neurons significantly reduces the survival of adult flies with a more severe effect in R1441C hLRRK2 flies suggesting increased neurotoxicity induced by this mutation during aging. To assess the effect of hLRRK2 expression on movement, we used a negative geotaxis test based on the ability of adult flies to climb the wall of a glass cylinder (35). We initially tested flies at 2 weeks of age and observe no difference between control and hLRRK2-expressing flies ($n = 60$). However, with advancing age, we observe a progressive loss of climbing ability in WT hLRRK2 flies with a more severe motor deficit in R1441C hLRRK2 flies, consistent with enhanced toxicity of the R1441C mutation in dopaminergic neurons (Fig. 1F).

WT and R1441C hLRRK2 expression induces dopaminergic neuronal loss in *Drosophila*

To evaluate pathogenic effects on dopaminergic neurons in hLRRK2-expressing flies, we monitored the number of tyrosine hydroxylase (TH)-positive dopaminergic neurons. In adult *Drosophila* brains, there are a number of dopaminergic neuronal clusters, such as the dorsolateral posterior protocerebral (PPL1), lateral posterior protocerebral (PPL2a/b), two dorsomedial posterior protocerebral clusters (PPM1/2 and PPM3), protocerebral anterior lateral (PAL) and protocerebral anterior medial (PAM) clusters (Fig. 1G) (36). We detect a significant and selective reduction of TH-positive neurons in the PPM1/2, PPL1, PAL and PPL2ab clusters in six week-old WT and R1441C hLRRK2 flies compared to control flies ($P < 0.01$) (Fig. 1H and I). Notably, R1441C hLRRK2 expression induces a more severe loss of dopaminergic neurons in the PPM1/2 and PPL1 clusters than WT hLRRK2, whereas both LRRK2 variants equivalently induce the complete loss of PAL and PPL2ab dopaminergic neurons (Fig. 1H and I). TH-positive neurons in the PAM and PPM3 clusters are not significantly altered in either of the two hLRRK2 strains. Our data indicates that specific subsets of dopaminergic neurons are selectively vulnerable to hLRRK2 expression in the *Drosophila* brain.

SILAC-based protein quantitation in flies overexpressing WT and R1441C hLRRK2

In good agreement with previous reports, our analyses demonstrate that WT and R1441C hLRRK2 overexpression in *Drosophila* induces robust dopaminergic neuronal loss and motor deficits therefore recapitulating key PD-like phenotypes (33). To further understand the pathogenic effects induced by hLRRK2 expression in dopaminergic neurons, we used quantitative proteomics to measure protein abundances in control and hLRRK2-overexpressing flies to provide a systematic proteome-wide analysis. To perform accurate and reliable protein quantification, we conducted a SILAC (stable isotope labelling of amino acids in cell culture)-based 'spike-in' approach using flies completely labelled with heavy $^{13}C_6$-lysine (Lys6) as an internal protein standard. Approximately 100 *Drosophila* heads from control and hLRRK2 transgenic strains as well as from Lys6-labelled SILAC flies were collected, and extracted proteins from the SILAC fly were mixed equally with protein extracts from each non-labelled fly strain (Fig. 2). SILAC labelling of flies was achieved by feeding flies with Lys6-labelled yeast for at least one fly generation (37). After tissue separation and protein extraction, we performed an in-solution digestion using the endoprotease LysC and analysed all samples with a quadrupole Orbitrap mass spectrometer. We measured three different time points (days 1, 10 and 30, $n = 3$) for each of control, WT and R1441C hLRRK2 flies. Each sample was measured for a 4 h gradient on 50 cm in-house packed columns coupled to a high resolution quadrupole Orbitrap mass spectrometer (QExactive) and data were analysed using the MaxQuant software package. This *single-shot* approach allowed us to profile 2 transgenic fly strains and 1 control fly strain at three different time points in triplicate in less than 4.5 days measurement time at an average protein quantification rate of 8.6 ± 0.8 protein quantifications/min. Approximately, 1.8 million MS/MS spectra were correlated to 31,035 unique peptide sequences resulting in the identification of 3,613 proteins. Reproducibility was determined by Pearson correlation coefficients between all experiments which were plotted on a heatmap using Euclidean distance and reveal that genotypes and time points show almost linear correlation ($r \sim 0.9$) and clear grouping (Supplementary Material, Fig. S1). For the hLRRK2 dataset including the appropriate control, ~2,000 proteins were quantified at each time point (days 1, 10 and 30) as a biological triplicate of control, WT and R1441C hLRRK2 flies demonstrating a strong overlap between LC-MS/MS runs (Supplementary Material, Table S1).

To initially determine the systematic effects of hLRRK2 overexpression in fly brain, we performed a principal component analysis covering >80% of the total variance by two components and find strong grouping of genotypes at each age (Fig. 3A). Interestingly, while WT hLRRK2 and control flies are closely associated with each other, the R1441C hLRRK2 flies reveal a clear segregation from other groups at all time points assessed indicating a distinct role for R1441C hLRRK2 in the development of PD-like phenotypes in flies. Additionally, we sought to

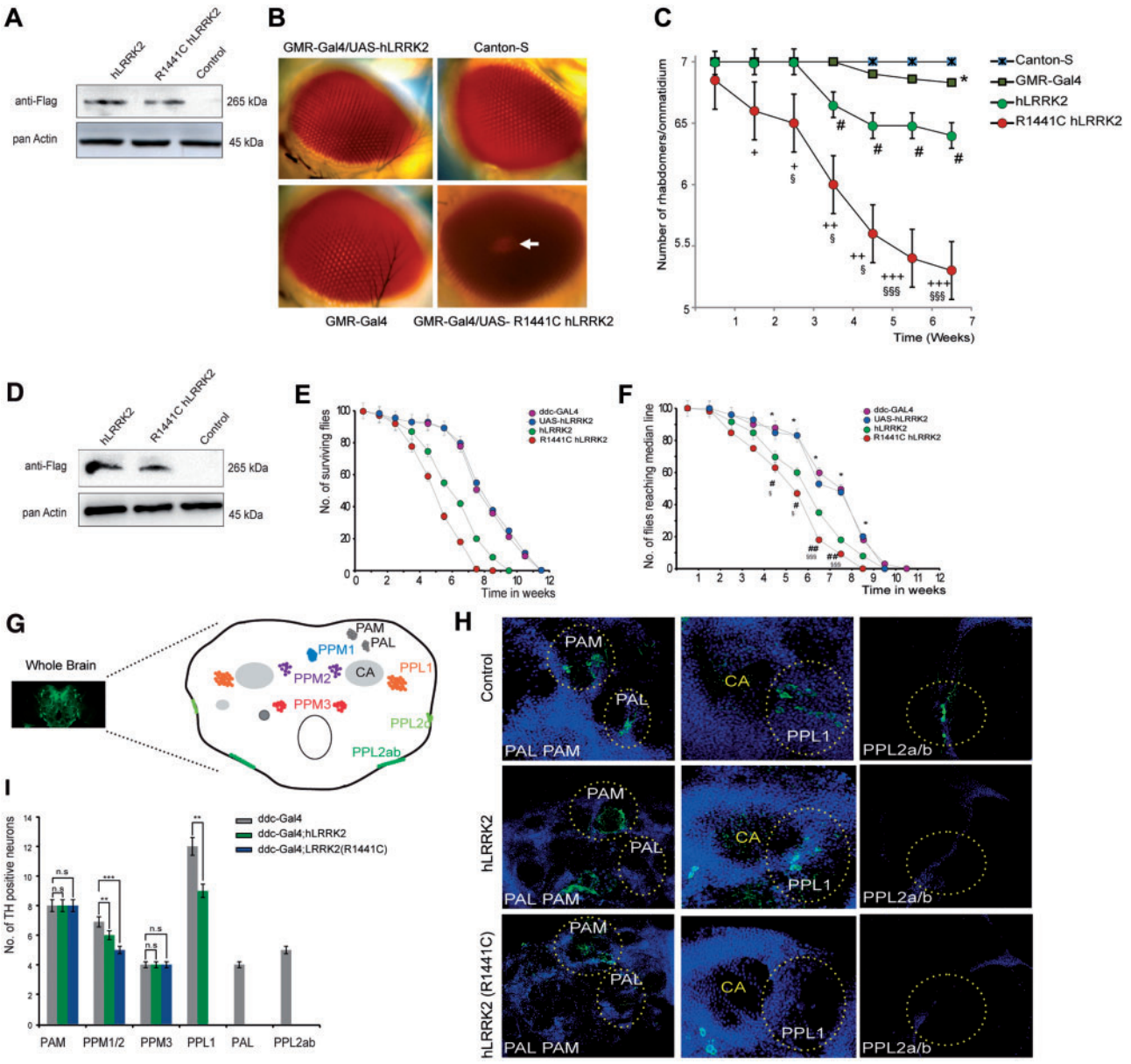

Figure 1. hLRRK2 overexpression caused retinal degeneration, locomotor dysfunction and degeneration of dopaminergic neurons in *Drosophila*. (**A**) Proteins were extracted from *Drosophila* heads and were subjected to western blot analysis with an anti-FLAG antibody. (**B**) White arrow marks the site of surface degeneration of ommatidial array. (**C**) The time course of photoreceptor degeneration determined by optical neutralization technique. Each data point was based on examination of >90 ommatidia from at least 6 flies. One-way ANOVA with Bonferonni post-hoc test. $^{*}P < 0.05$ Canton-S vs GMR-Gal4, $^{\#}P < 0.05$ GMR-Gal4 vs. hLRRK2 (Wt), $^{+}P < 0.05$, $^{++}P < 0.01$, $^{+++}P < 0.005$ GMR-Gal4 vs. hLRRK2 (R1441C), $^{\S}P < 0.05$, $^{\S\S\S}P < 0.01$ hLRRK2 (Wt) vs hLRRK2 (R1441C). (**D**) Proteins were extracted from *Drosophila* heads and western blot analysis was performed with an anti-FLAG antibody and confirmed FLAG-hLRRK2 protein expression in ddc-driven transgenic flies. (**E**) Survival curves of flies ($n = 50$) expressing either WT or R1441C hLRRK2. ddc-Gal4 driven R1441C hLRRK2 expression causes shorter lifetime (red circles). (**F**) 50 flies were subjected to climbing assay. One-way ANOVA with Bonferonni post-hoc test is indicated by $^{*}P < 0.05$ UAS-LRRK2 vs ddc-Gal4, $^{\#}P < 0.05$, $^{\#\#}P < 0.01$ ddc-Gal4 vs hLRRK2 (R1441C)). $^{\S}P < 0.05$, $^{\S\S\S}P < 0.01$ hLRRK2 vs hLRRK2 (R1441C). (**G**) A schematic overview of different dopaminergic clusters in the fly brain and (left) whole-mount tyrosine hydroxylase (TH) staining with a mouse anti-TH antibody. (**H**) Degeneration of dopaminergic neurons in different dopaminergic clusters. Posterior protocerebral (PPL1 and PPL2a/b) cluster and protocerebral anterior medial (PAM). (**G**) Quantification of TH-positive neurons in WT hLRRK2, R1441C hLRRK2 and a ddc-Gal4 control in 6 week-old flies. Dorsolateral posterior protocerebral (PPL1) and dorsomedial posterior protocerebral (PPM1/2) clusters show statistically significant differences between ddc-Gal4, WT hLRRK2 and R1441C hLRRK2 flies that are indicated: $^{**}P < 0.01$, $^{**}P < 0.005$ one-way ANOVA with Bonferonni post-hoc test.

determine if the drivers that are responsible for this clear segregation effect are enriched in KEGG pathways and identified 'G-protein coupled signalling', 'Parkinson's disease', and 'Synapse part' as contributing to this effect (Fig. 3B). Our data suggest that WT hLRRK2 and R1441C hLRRK2 expression induce distinct molecular signatures in the fly brain at different time points. To identify proteins that are differentially expressed in R1441C hLRRK2 flies compared to WT hLRRK2 flies, we utilized a two-sided t-test with correction for multiple testing problems by a randomization-based FDR calculation. We identify 132, 227 and 304 differentially-expressed proteins between WT hLRRK2 and R1441C hLRRK2 at 1, 10 and 30 days, respectively, at an FDR cutoff of 1% (Fig. 3C–E). Next, we asked whether a majority of proteins acting in the same pathways/compartments are

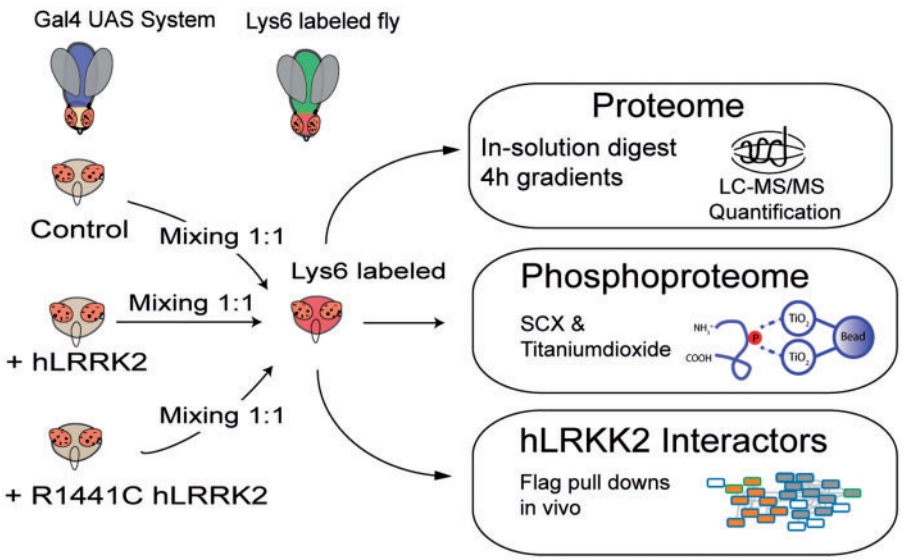

Figure 2. Experimental workflow for SILAC-based protein quantification. The left side represents the hLRRK2-overexpressing fly strains. The SILAC fly mixture consists of a pool of flies from 1, 10 or 30 day-old Lys6-labelled fly heads and was used as a spike-in standard for accurate protein quantification. Protein mixtures from labelled (red head) and unlabelled flies (brown head) were subjected to in-solution digestion, phosphopeptide enrichment and protein–protein interaction studies.

similarly regulated by performing 1D enrichment on the log2 ratios of R1441C hLRRK2 versus WT hLRRK2 (38). By plotting the mean of identical annotated proteins for R1441C hLRRK2/WT hLRRK2 against the enrichment score, we detect an up-regulation of proteins involved in metabolic pathways such as 'lysine degradation', 'glycolysis/gluconeogenesis' and 'fatty acid metabolism' as well as important core complexes including the 'proton-transporting ATP synthase complex' in R1441C hLRRK2 flies (Fig 3F). Moreover, we observe a down-regulation in R1441C hLRRK2 flies of signalling pathways such as the G-protein coupled receptor signalling pathway, GnRH (gonadotropin-releasing hormone) signalling pathway and inaD (Inactivation no afterpotential D, phototransmission) signalling complex as well as a reduction in abundance of proteins participating in neurotransmitter transport, axon guidance, synaptic vesicle formation and SNARE interaction in vesicular transport (Fig. 3F).

Synaptic vesicle (SV) recycling is an important step for neurotransmitter release and the activation of post-synaptic receptor channels. Three key proteins, synaptobrevin, syntaxin 1A and SNAP-25, form the core of the SNARE complex (soluble attachment NSF protein receptor) that mediates synaptic vesicle formation and exocytosis (39). Dysregulation of syntaxin 1A and synaptobrevin in flies lead to defects in neurotransmission and deficiency in SNAP-25 (synaptosome-associated protein 25 kDa) is associated with human neurological disorders (40,41). Here, we find two core SNARE proteins, SNAP-25 and syntaxin 1A, to be down-regulated in R1441C hLRRK2 compared to WT hLRRK2 and control flies (Fig. 3E, Supplementary Material, Table S1). Similarly, the exocytosis-related protein synaptotagmin-1 (Syt1) and the Ras-related protein Rab3 are selectively decreased in R1441C hLRRK2 flies at day 30. Of note, a loss of Syt1 was reported in the hippocampus of Alzheimer's disease patients (42). Therefore, we speculate that R1441C hLRRK2 expression induces the down-regulation of specific SV proteins that could lead to the dysregulated SV formation and recycling most likely resulting in synaptic dysfunction in dopaminergic neurons.

The R1441C mutation in LRRK2 in knockin mice leads to an inhibition of dopamine and catecholamine synthesis in cultured adrenal chromaffin cells (43). In *Drosophila* brain, we identify three down-regulated proteins, including punch (GTP cyclohydrolase), purple (6-pyruvoyl tetrahydrobiopterin synthase) and henna, all involved in dopamine synthesis in flies. Protein henna is a phenylalanine hydroxylase that catalyzes phenylalanine conversion to tyrosine, the major substrate for dopamine and other catecholamines. In addition, these three proteins are down-regulated most apparently on day 10 in R1441C hLRRK2 compared to WT hLRRK2 and control flies (Fig. 3D and E, Supplementary Materials, Table S1, Fig. S2), potentially suggesting that this time point is crucial for the development of PD phenotypes. GTP cyclohydrolase (GCH1) and 6-pyruvoyl tetrahydrobiopterin synthase (PTS) are important enzymes for the synthesis of tetrahydrobiopterin (BH4) an essential cofactor for the neurotransmitter-synthesizing enzyme tyrosine hydroxylase, phenylalanine hydroxylase and tryptophan hydroxylase. Defects in BH4 metabolism cause monoamine-related neurotransmitter diseases resulting in dopamine-responsive dystonia (DRD) with a movement disorder and Parkinsonian features (44,45). Collectively, our data reveal a clear link between increased expression of R1441C hLRRK2 and several enzymes involved in dopamine biosynthesis.

Another down-regulated enzyme in our model is Tan, which converts N-beta-alanyl dopamine (NBAD) to beta-alanine and dopamine. Flies lacking Tan have disturbed dark pigmentation due to reduced dopamine and melanin levels in the skin. Tan function is also crucial for light detection by converting carcinine to histamine and β-alanine (46). Here we find a significant two-fold reduction of Tan in R1441C hLRRK2 flies compared to WT hLRRK2 and control flies at day 30. Of note, this protein is also significantly down-regulated in WT hLRRK2 flies at day 10 but unchanged in WT hLRRK2 versus control animals at day 30. We could verify reduced Tan levels in *Drosophila* brains by Western blotting and immunohistochemistry on cryosections with an anti-Tan antiserum, and we show representative SILAC pairs for Tan peptides (Fig. 3G-I). These data suggest that the consistent down-regulation of Tan in R1441C hLRRK2 flies could be an important factor for the development of PD. The expression of the general neuronal marker protein Bruchpilot (nc82) is not altered between the different fly strains. Conversely, 133

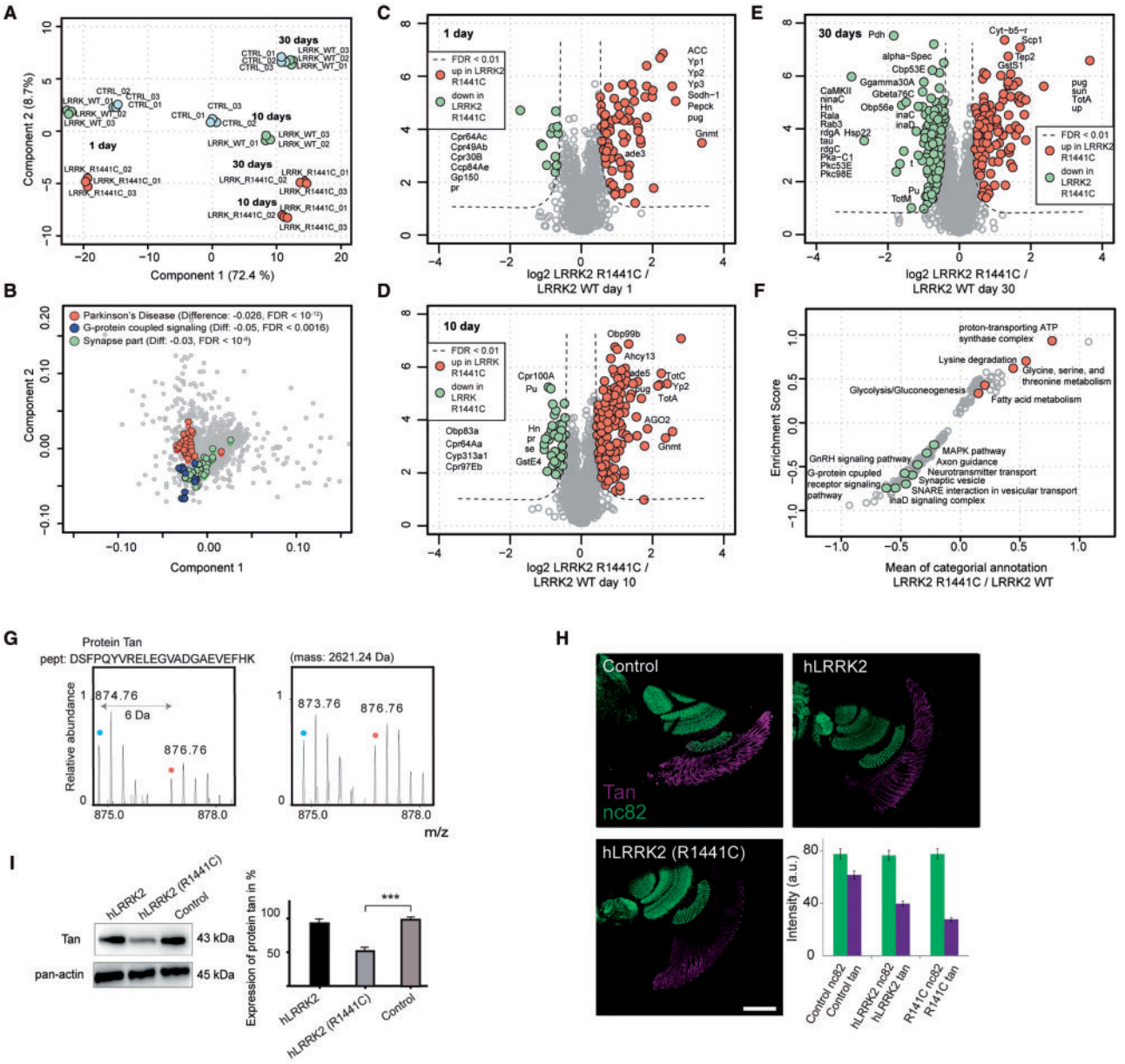

Figure 3. Systematic characterization of R1441C hLRRK2 overexpression. **(A)** Principal component analysis of control, WT hLRRK2 and R1441C hLRRK2 at 1, 10 and 30 days showing clear group segregation of R1441C hLRRK2 versus control and WT hLRRK2 flies at all time points. **(B)** Drivers of component 1 and 2 in the PCA analysis, indicating that proteins annotated with PD (KEGG), Synapse part (GOCC) and G-protein-coupled signalling (GOBP), are jointly responsible for the described difference between genotypes. FDR was calculated by Benjamini-Hochberg (BH) correction. Volcano plots using a permutation-based FDR cutoff of 0.01 reveal 73 significantly different expressed proteins at day 1 **(C)**, 189 at day 10 **(D)**, and 346 at day 30 **(E)**. **(F)** 1D enrichment along the log2 ratio between R1441C LRRK2 versus WT LRRK2 at day 30 indicates that proteins of several signalling pathways are found to be downregulated in R1441C LRRK2 strain (down left) while upregulation was found for proteins participating in metabolism (right top). The BH-FDR cutoff was set to 0.02. **(G)** MS spectra of peptide sequences identified for Tan protein. **H)** Immunostaining of tan (violet) and bruchpilot (antibody nc82; green) of *Drosophila* head sections. Scale bar: 100 μm. **(I)** Western blots showed the down regulation of Tan protein in R1441C hLRRK2 flies compared to control and WT hLRRK2 flies. Quantification ($n = 3$) of Tan protein signals in R1441C hLRRK2 flies. Bars indicate mean ± SEM. ***$P < 0.0001$ by one-way ANOVA with Dunnett's multiple comparison test.

proteins show a significant up-regulation in R1441C hLRRK2 flies compared to WT hLRRK2 at 30 days (Fig. 3D and E, Supplementary Material, Table S1). For example, we observe several proteins associated with the actin cytoskeleton and factors regulating oxidative stress. The identification of the two actins (Act88F, Act79B) with increased levels supports the association of R1441C hLRRK2 with cytoskeletal actin filaments (47). Oxidative stress is associated with PD and it has been shown that gluthatione-S-transferases function as a cellular defence against toxic agents and radicals (48). Here, we observe a clear up-regulation of GstS1 in aged flies overexpressing R1441C hLRRK2, potentially indicating an adaptive compensatory mechanism to protect cells from oxidative stress in response to neurodegeneration.

Taken together, our SILAC-based quantitative mass spectrometric approach reveals time-dependent protein changes in flies overexpressing R1441C hLRRK2 compared to age-matched control flies and provides a comprehensive database for the study of PD in *Drosophila* models expressing mutant and wild-type versions of PD-related proteins. Moreover, our dataset

reveals an association of specific proteins involved in synaptic vesicle recycling to be altered selectively in the R1441C hLRRK2 fly brain suggesting a specific disease mechanism for the R1441C mutation.

Overexpression of WT and R1441C hLRRK2 cause different patterns of protein changes during aging

To provide additional insight into the mechanisms of neurotoxicity induced by WT and R1441C LRRK2, we used the 1D enrichment strategy of GO-terms and KEGG categories to identify pathways that are differentially-regulated between WT and R1441C hLRRK2 flies (Fig. 3B, F). Mitochondria are important not only for energy production but are also essential for regulating cellular stress responses, calcium homeostasis and apoptosis (49). Moreover, it has been shown that the G2019S mutation in LRRK2 results in reduced intracellular ATP levels due to impaired mitochondrial function in patient-derived human fibroblasts (50). Here, we detect the up-regulation of several subunits of the ATP synthase (complex V) in WT and R1441C hLRRK2 flies, suggesting that mitochondrial function might be disturbed in aged hLRRK2 flies (Fig. 4A).

Next, we focused on the gene ontology term for transmission of nerve impulses (GO: 0019226, $n = 26$) which contains a number of proteins that are clearly down-regulated in R1441C hLRRK2 flies (Fig. 3F). Since a fraction of hLRRK2 localizes to synapses and may play an important role in synaptic vesicle endocytosis (25,51), we performed a box plot analysis to compare the ratios of synaptic proteins between WT hLRRK2 and R1441C hLRRK2 flies in comparison to control flies during aging. Log2 transformed SILAC ratios of R1441C hLRRK2 and WT hLRRK2 reveal a clear reduction of the synapse-associated protein (Sap47), synaptotagmin-1 (Syt1) and the calcium-binding protein Frequinin-1 (Frg1) in R1441C hLRRK2 flies (Fig. 4B). Frequinin plays a role in neurite outgrowth and inactivation of Frg1 alters synaptic transmission (52). Of note, the analysis of WT hLRRK2 flies reveals no effect on synaptic vesicle proteins.

G-protein-coupled receptor (GPCR) signalling is linked to the pathobiology of PD. It has been shown that serine-129 phosphorylation of α-synuclein induced by G protein-coupled receptor kinases (GRK3, 5, 6) enhance the ability of membrane-associated α-synuclein to increase dopamine uptake (53). Moreover, the GRK6-dependent phosphorylation of α-synuclein enhances the formation of Lewy body-like inclusions and induces the degeneration of dopaminergic neurons (54). Here, we used the KEGG category of GPCR-associated proteins and plotted them for each hLRRK2 fly strain between days 1 to 30 (Fig. 4C). In total, we identify 31 GPCR-related proteins and for the majority of the quantified proteins (25 from 27 in total) a clear down-regulation is detected in R1441C hLRRK2 compared to WT hLRRK2 flies, suggesting a potential relationship between R1441C hLRRK2 activity and GPCR signalling.

In the class of proteins containing a protein kinase domain (PFAM: PF00069), we identify 76 kinases and our analysis reveals a significant down-regulation ($P < 0.00002$) of quantified kinases in R1441C hLRRK2 flies compared to WT hLRRK2 flies at day 30 (Fig. 4D). Casein kinase II phosphorylates soluble α-synuclein at Ser-129 which leads to enhanced neurotoxicicty and inclusion formation in *Drosophila* (55). In our R1441C hLRRK2 fly model, we detect a significant down-regulation of casein kinase II alpha subunit during aging, suggesting a reduced phosphorylation of target proteins. Protein kinase C isoforms have previously been nominated as potential therapeutic targets for various diseases, including cancer, heart failure and PD (56). Similar to GPCR signalling proteins, the detected kinases including two protein kinase C isoforms, are down-regulated in R1441C hLRRK2 flies compared to WT hLRRK2 flies.

Together, the expression of R1441C hLRRK2 in the *Drosophila* brain induces a distinct protein pattern compared to all other tested fly strains and we observe a clear age-dependent effect of R1441C hLRRK2 on GPCR signalling proteins and several PD-related protein kinases.

Global phosphoproteome analysis of *Drosophila* expressing hLRRK2 variants

To further elucidate the function of hLRRK2 kinase activity during the degeneration of dopaminergic neurons, we elected to analyse and compare the global phosphoproteome of control, WT hLRRK2 and R1441C hLRRK2 flies at day 30. Similar to the proteome analysis, we used a SILAC-based fly approach as an internal protein standard for accurate phosphopeptide quantification and performed a biological triplicate for each fly strain ($n = 3$). Extracted proteins from head tissue (~2–3 mg) were digested in-solution and we utilized a combination of strong cation exchange chromatography (SCX) and titanium dioxide affinity to enrich for phosphorylated peptides. Each fraction was analysed by 2.5 h liquid chromatography gradients and measured with a quadrupole Orbitrap mass spectrometer. In total, we identified 5,449 phosphorylation sites and detected 4,142 class I (localization prob. >0.75, Score diff >5) phosphosites (Supplementary Material, Table S2). Among the class I phosphorylation sites, we quantified 2,529 phosphosites in at least two out of three experiments (Supplementary Material, Table S3). Similar to previous studies, we observed 83% serine, 16% threonine and <1% tyrosine phosphorylation sites. Good reproducibility of our quantitative phosphoproteome is indicated by Pearson correlations for direct ratios comparing WT hLRRK2, R1441C hLRRK2 and control flies (Fig. 5A and C). Clustering of these ratios using Euclidean distances results in clear grouping of the three biological replicates for each fly strain (Fig. 5A). Notably, after normalization to total protein levels we observe 19 and 26 regulated phosphosites in WT hLRRK2 and R1441C hLRRK2, respectively, compared to control flies (Supplementary Material, Table S2). A direct comparison of both hLRRK2 fly strains reveals the increased phosphorylation at 22 sites in R1441C hLRRK2 flies. For example, recent studies demonstrated that LRRK2 phosphorylates the microtubule-associated protein Futsch (33). Our phosphoproteome analysis confirms Futsch phosphorylation and in addition, we quantified enhanced site-specific phosphorylation at positions pS4106 (~10-fold) and pS4909 (~1.5-fold) in R1441C hLRRK2 compared to WT hLRRK2 flies (Fig. 5C and D). In addition, Futsch co-localizes with Ankyrin2 an essential component of the cytoskeleton, which stabilizes the formation of synaptic microtubules (57). Here, we identified several Ank2 phosphorylation sites and the pS11169 site at the C-terminus of Ank2 is highly conserved between fly and humans (Fig. 5E).

Next, we quantified several phosphorylation sites on synaptic vesicle proteins, including the presynaptic protein synaptojanin-1 (Synj), a polyphosphoinositide phosphatase that is localized in motor neuron synapses and promotes synaptic vesicle (SV) uncoating during endocytosis (58,59). Interestingly, we observe a significant increase in synaptojanin-1 phosphorylation at pT1131 and pS1142 in R1441C hLRRK2 flies (Supplementary Material, Fig S3). Moreover, it has been

A

	Uniprot ID	Protein names	Gene names	Peptides	Sequence coverage [%]	-Log t-test p value R1441C hLRRK2 vs hLRRK2 day30	log2 ratio R1441C hLRRK2 vs hLRRK2 day30
mitochondrial proton-transport ATP synthase complex	Q8IR24			6	98.2	3.53	0.61
	Q24407	ATP synthase-coupling factor 6	ATPsyn-Cf6	12	60.4	5.19	0.70
	Q24251	ATP synthase subunit d,	ATPsyn-d	18	80.9	6.06	0.76
	Q94516	ATP synthase subunit b	ATPsyn-b	20	69.5	4.98	0.69
	O77134		ATPsynE	12	100	4.53	0.83
	Q9VKM3		ATPsynG	3	52.5	2.31	0.87

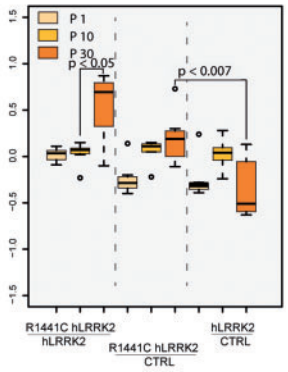

B

	Uniprot ID	Protein names	Gene names	Peptides	Sequence coverage [%]	-Log t-test p value R1441C hLRRK2 vs hLRRK2 day30	log2 ratio R1441C hLRRK2 vs hLRRK2 day30
Transmission of nerve impulse	P37236	Frequenin-1	Frq1	9	46	2.52	-0.53
	Q960T2	Synapse-ass. protein of 47 kDa	Sap47	12	40.4	2.50	-0.52
	P36975	Synaptosomal-ass. protein 25	Snap25	7	44.8	4.19	-0.71
	E1JJ35	Complexin	cpx	16	78.9	3.78	-0.48
	P21521	Synaptotagmin 1	Syt1	17	39.8	3.13	-0.49
	E1JJA5	Dynamin	shi	36	55.6	3.94	-0.49
	P46461	Vesicle-fusing ATPase 1	comt	42	66.6	2.92	-0.52
	P13395	Spectrin alpha chain	alpha-Spec	138	72.5	6.49	-0.44
	Q00963	Spectrin beta chain	beta-Spec	116	64	5.00	-0.44
	E1JIS7	Peripheral membrane protein CASK	CASK	11	15.6	1.54	-0.51
	P40417	Mitogen-activated protein kinase ERK-A	rl	8	28.5	1.00	-0.43

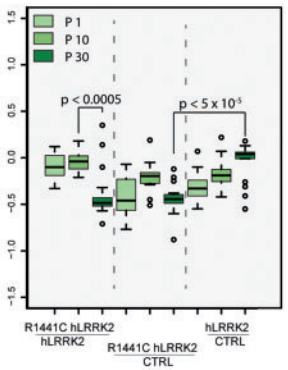

C

	Uniprot ID	Protein names	Gene names	Peptides	Sequence coverage [%]	-Log t-test p value R1441C hLRRK2 vs hLRRK2 day30	log2 ratio R1441C hLRRK2 vs hLRRK2 day30
GPCR downstream signaling	P13677	Protein kinase C, eye isozyme	inaC	24	50.6	4.66	-0.70
	P10676	Neither inac. nor afterpot. protein C	ninaC	47	44.8	3.35	-0.48
	Q9VU58	Neuropeptide-like 2	Nplp2	5	50	2.88	-0.53
	Q09103	Eye-specific diacylglycerol kinase	rdgA	20	26.6	3.58	-0.79
	E1JHC3	Guanine nucleotide-binding prot.	Ggamma30A	10	91.7	5.75	-1.00
	P23625	G protein alpha q subunit	Galphaq	19	66.6	3.68	-0.87
	P29829	Guanine nucleotide-binding prot.	Gbeta76C	16	53.8	5.39	-1.02
	P16378	G protein alpha o subunit	Galphao	16	57.3	4.96	-0.50
	P56079	Phosphatidate cytidylyltransferase	CdsA	11	22.8	4.17	-0.44
	P19334	Transient receptor potential protein	trp	39	37.2	4.06	-0.76
	Q24008	Inact.-no-after-potential D protein	inaD	39	78.9	4.38	-0.74
	E1JJD5	Phosphoinositide phospholipase C	norpA	61	59.5	4.54	-0.71
	P20354	G protein alpha s subunit	Galphas	15	62	2.35	-0.51
	P61849	Dromyosuppressin	Dms	2	35	4.99	-1.51

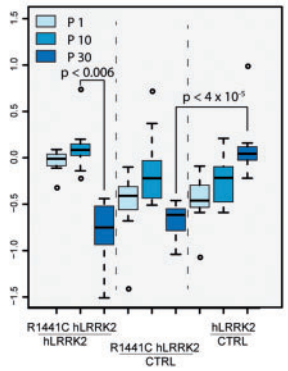

D

	Uniprot ID	Protein names	Gene names	Peptides	Sequence coverage [%]	-Log t-test p value R1441C hLRRK2 vs hLRRK2 day30	log2 ratio R1441C hLRRK2 vs hLRRK2 day30
P_Kinases PFAM domain	A4V3W2	Protein kinase shaggy	sgg	12	30.4	2.81	-0.43
	P13678	Protein kinase C	Pkc98E	13	22.1	2.36	-0.78
	P05130	Protein kinase C, brain isozyme	Pkc53E	17	28.2	3.39	-0.64
	P12370	cAMP-dep. prot. kinase cat. subunit	Pka-C1	15	54.1	3.24	-0.57
	Q7KSD3		fray	11	30.8	2.81	-0.39
	A4V2B8	Casein kinase II subunit alpha	CkIIalpha	9	53.3	1.45	-0.44
	A4V134	Calcium/calmodulin-dep. prot. kinase type II alpha chain	CaMKII	27	52.8	3.19	-0.49

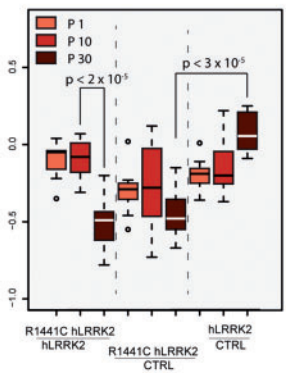

Figure 4. R1441C hLRRK2-induced PD is regulated by distinct groups of proteins. (**A**) Selection of proteins of the mitochondrial proton transport system and box plot series for multiple comparisons between all genotypes. Box plots represent the log2 direct ratio distribution of proteins annotated with the specific term. (**B**) Differences in abundance level of proteins of the KEGG pathway—*transmission of nerve impulse*. (**C**) Altered protein expression of proteins contributing in *G-protein coupled signalling*. (**D**) Proteins with the kinase PFAM domain are significantly down-regulated in R1441C hLRRK2-overexpressing flies compared to WT hLRRK2 flies. Note that proteins carrying kinase domain were excluded from the analysis of the *G-protein coupled signalling* members. *P* values were calculated by the Wilcoxon Rank test.

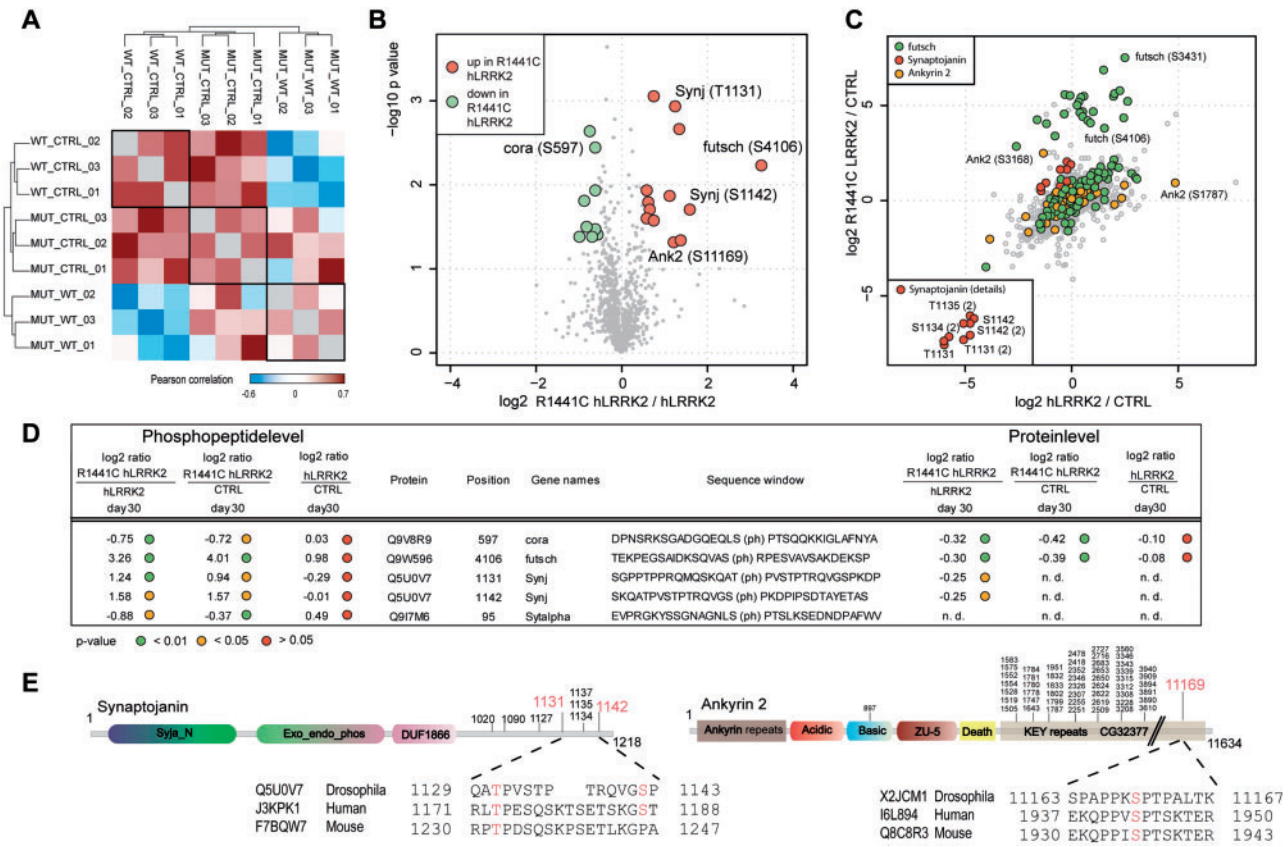

Figure 5. Phosphoproteomics reveals increased phosphorylation of synaptic vesicle proteins. **(A)** Hierarchical clustering of the correlation matrix determined by Pearson correlation of triplicates indicates differences between R1441C hLRRK2 and WT hLRRK2. Note that these values are calculated based on the direct ratio and not the raw SILAC ratio. **(B)** Volcano plot of R1441C hLRRK2 versus WT hLRRK2 fly strain. Significance was considered for p-values below 0.05 and fold changes greater than 1.5. **(C)** Scatter plot of log2 transformed direct ratios between R1441C hLRRK2 and WT hLRRK2 versus control flies. Phosphorylation sites of ankyrin 2, synaptojanin and futsch are colour coded and show strong upregulation of phosphorylation sites in flies overexpressing R1441C hLRRK2. **(D)** Selected list of significantly regulated phosphopeptides with their modified sequence and protein quantification. P-values are colour coded from a two-sided *t*-test. **(E)** Sequence alignment of regulated phosphopeptides of *Drosophila* synaptojanin and ankyrin 2 to the human and mouse protein sequences.

demonstrated that synaptojanin-1 mutations in flies lead to impaired endocytosis and disrupted vesicle recycling, whereas homozygous mutations in *SYNJ1* (i.e. R258Q) cause early-onset, autosomal recessive familial PD (*PARK20*) most likely due to defective recycling of synaptic vesicles (60,61). Notably, a sequence alignment of fly, mouse/rat and human synaptojanin-1 protein sequence reveals conservation of the fly T1131 phospho-site (T1173 in human) and recent global phosphorylation studies also indicate that synaptojanin-1 is phosphorylated at the corresponding site, T1173 (Uniprot: J3KPK1) in humans (62) as well as pT1217 (Uniprot: Q62910) in rats (63) (Fig. 5E). Therefore, we suggest that the pT1131 phosphorylation site of synaptojanin-1 might be a direct target of R1441C hLRRK2 kinase activity in *Drosophila*. Moreover, our data indicate that the R1441C mutation within the Roc GTPase domain of hLRRK2 results in enhanced kinase activity compared to WT hLRRK2 in the *Drosophila* brain. In contrast, the membrane-trafficking and calcium sensor, synaptotagmin-1 alpha (Syt1, isoform A), exhibits reduced phosphorylation at pS95 in R1441C hLRRK2 flies compared to control flies. However, since Syt1 is not detectable at the protein level, a normalization for this phosphorylation site is not possible (Fig. 5D).

Phosphorylation of human synaptojanin-1 by hLRRK2 *in vitro*

Next, we examined whether WT and R1441C hLRRK2 variants can directly phosphorylate human synaptojanin-1 using *in vitro* radioactive kinase assays. The conservation of the T1131 site on synaptojanin-1 and its known phosphorylation in flies, mouse/rat and humans potentially suggests a conserved mechanism to regulate the activity of synaptojanin-1 via LRRK2 kinase activity under normal and pathological conditions. To initially confirm the phosphorylation of human synaptojanin-1 by hLRRK2, we combined recombinant GST-tagged hLRRK2 (WT, R1441C and kinase-inactive D1994A; residues 970-2527) with recombinant GST-tagged full-length human SYNJ1 and [^{33}P]-γ-ATP in the presence or absence of LRRK2-IN-1, a specific LRRK2 kinase inhibitor. Both WT and R1441C LRRK2 are able to efficiently and robustly phosphorylate SYNJ1 *in vitro* whereas treatment with LRRK2-IN-1 inhibits LRRK2-mediated SYNJ1 phosphorylation in a dose-dependent manner (Supplementary Material, Fig. S4A and B). As expected, kinase-inactive D1994A LRRK2 fails to induce SYNJ1 phosphorylation (Supplementary Material, Fig. S4C). To further confirm and quantify human SYNJ1 phosphorylation

by LRRK2 variants, *in vitro* kinase assays were conducted using soluble, recombinant full-length FLAG-tagged human LRRK2 (WT, R1441C, G2019S and D1994A) and FLAG-tagged human SYNJ1 (residues 1-1350; brain-specific 145 kDa isoform) that were immunopurified from transiently transfected HEK-293T cells using anti-FLAG-M2-sepharose (64). Importantly, we observe the direct and robust phosphorylation of SYNJ1 by WT, R1441C and G2019S LRRK2 compared to D1994A LRRK2 (Fig. 6A). Quantitation of SYNJ1 phosphorylation normalized to total SYNJ1 reveals enhanced phosphorylation by G2019S LRRK2 (~2-fold) relative to WT and R1441C LRRK2, which both phosphorylate SYNJ1 at similar levels (Fig. 6B). Notably, in contrast to *Drosophila* brain, R1441C hLRRK2 does not enhance SYNJ1 phosphorylation relative to WT hLRRK2 *in vitro* (Fig. 6B), similar to the reported impact of the R1441C mutation on the phosphorylation of Rab8a, ArfGAP1 and other substrates *in vitro* (14,28). We next conducted similar *in vitro* kinase assays with non-radioactive ATP and measured the phosphorylation of recombinant GST-tagged human SYNJ1 and LRRK2 variants by mass spectrometry. We can confirm the phosphorylation of human SYNJ1 (Uniprot: J3KPK1) at position pT1173 (equivalent to fly pT1131) by WT and R1441C LRRK2 (Fig. 6C and D). D1994A LRRK2 does not appreciably increase phosphorylation of SYNJ1 at T1173 within a 60 min incubation time (Fig. 6C and D). Notably, we detect a total of six phosphorylation sites in LRRK2 by mass spectrometry and four of these sites (pT1343, pT1348, pT1452, pT1503) exhibit an increased intensity after a 60 min incubation with non-radioactive ATP. All phosphorylation sites were localized within the Roc domain confirming the strong autophosphorylation activity of WT and R1441C hLRRK2 in these *in vitro* kinase assays (Supplementary Material, Table S4) (65,66).

Immunoprecipitation of hLRRK2 from *Drosophila* brain identifies interactions with synaptic proteins

Since the integrative proteome and phosphoproteome analysis of hLRRK2 fly models reveals a functional correlation with synaptic vesicle trafficking we conducted co-immunoprecipitation (IP) assays of FLAG-tagged hLRRK2 protein from fly brain to determine a potential interaction with SV proteins. IP experiments were performed using an anti-FLAG antibody to enrich for potential binding partners of hLRRK2. To distinguish between authentic protein interactors and non-specific binding, we used protein extracts from *ddc-gal4* flies as a control. Mass spectrometric analysis and label-free protein quantification of biological duplicate experiments reveal 138 putative interactors (FDR <0.05, log2 fold change >0.58) including several known LRRK2 binding partners, such as Rab3, Rab5, synapsin and vesicle fusing protein (Nsf2) (51) (Fig. 6E, Supplementary Material, Table S4). These interactors reflect the association of LRRK2 with synaptic vesicle formation and highlight the sensitivity of our IP experiments. Moreover, we are able to identify synaptojanin-1 as an interaction partner of hLRRK2 as well as EndoA that is highly enriched in IP experiments compared to control IPs (no antibody) ($P = 0.17$) therefore providing additional evidence for a functional interaction of hLRRK2 and synaptojanin-1. A known hLRRK2 interactor is dynamin-1, a protein that mediates membrane scission during endocytosis (26), and here we identify the *Drosophila* ortholog Shi as a significantly enriched interactor. Therefore, our quantitative protein-protein interaction study in fly brain for hLRRK2 reveals a physical interaction with several synaptic vesicle proteins and supports an important role for hLRRK2 as a kinase responsible for the phosphorylation of synaptic vesicle proteins.

Discussion

To gain a better understanding of the pathobiology of neurodegenerative diseases, several useful model organisms, including yeast, worms, flies and rodents, have been established by overexpressing a human gene and its disease-associated variant (67).

Our study convincingly demonstrates that overexpression of WT or R1441C hLRRK2 in flies induces a severe degeneration of retinal and dopaminergic neurons, reduced survival and locomotor impairment compared to age-matched controls. Following the expression of hLRRK2 selectively in dopaminergic neurons, we observe impaired locomotor activity that strongly correlates with a significant reduction of neurons in several well-characterized dopaminergic clusters in the fly brain. Moreover, consistent with previous studies, we also observe a more severe phenotype in flies overexpressing R1441C hLRRK2 compared to the WT protein, confirming the enhanced neurotoxicity of the R1441C mutation. Interestingly, certain dopaminergic neuronal clusters were resistant to the neurotoxic effects of hLRRK2 expression in transgenic flies. This might reflect different expression levels of the Gal4 activator protein within individual dopaminergic clusters, and therefore different levels of hLRRK2 expression. Alternatively, subpopulations of dopaminergic neurons might have different susceptibility to hLRRK2-induced toxicity. Taken together, this work supports the observation that the overexpression of WT or R1441C hLRRK2 results in the degeneration of dopaminergic neurons leading to PD-related phenotypes in flies.

Although several studies have employed the overexpression of hLRRK2 variants to investigate disease-related mechanisms in various model systems, until now there is a paucity of studies using large-scale proteomic profiling approaches in order to evaluate global protein dynamics in the brains of living organisms. In the present study, we provide an unbiased and accurate quantitative large-scale screening of WT and R1441C hLRRK2 fly brains to distinguish between physiological and pathophysiological changes at the proteome and phosphoproteome level. Moreover, to provide insight into how the R1441C mutation in the GTPase domain of LRRK2 alters its kinase activity and to identify its potential phosphorylation targets, we analysed the brain phosphoproteome from 30 day-old control flies compared with transgenic flies expressing WT or R1441C hLRRK2. For the first time, our data provide a comprehensive catalogue of the quantitative changes in the brain phosphoproteome that occur in new *Drosophila* hLRRK2 models of PD that will provide critical mechanistic insight into the neurotoxic actions of familial *LRRK2* mutations.

R1441C hLRRK2 overexpression results in dysregulation of synaptic vesicle proteins

Our temporal proteomic screening in living flies revealed a significant regulation of 346 proteins after 30 days in R1441C hLRRK2 flies compared to WT hLRRK2 flies at an FDR of 0.01. This clearly indicates that the R1441C mutation with reduced GTPase activity leads to robust protein changes during aging. LRRK2 has been suggested to play a role in modulating mitochondrial dynamics and activity. For example, a proportion of LRRK2 is localized to the mitochondrial outer membrane in the

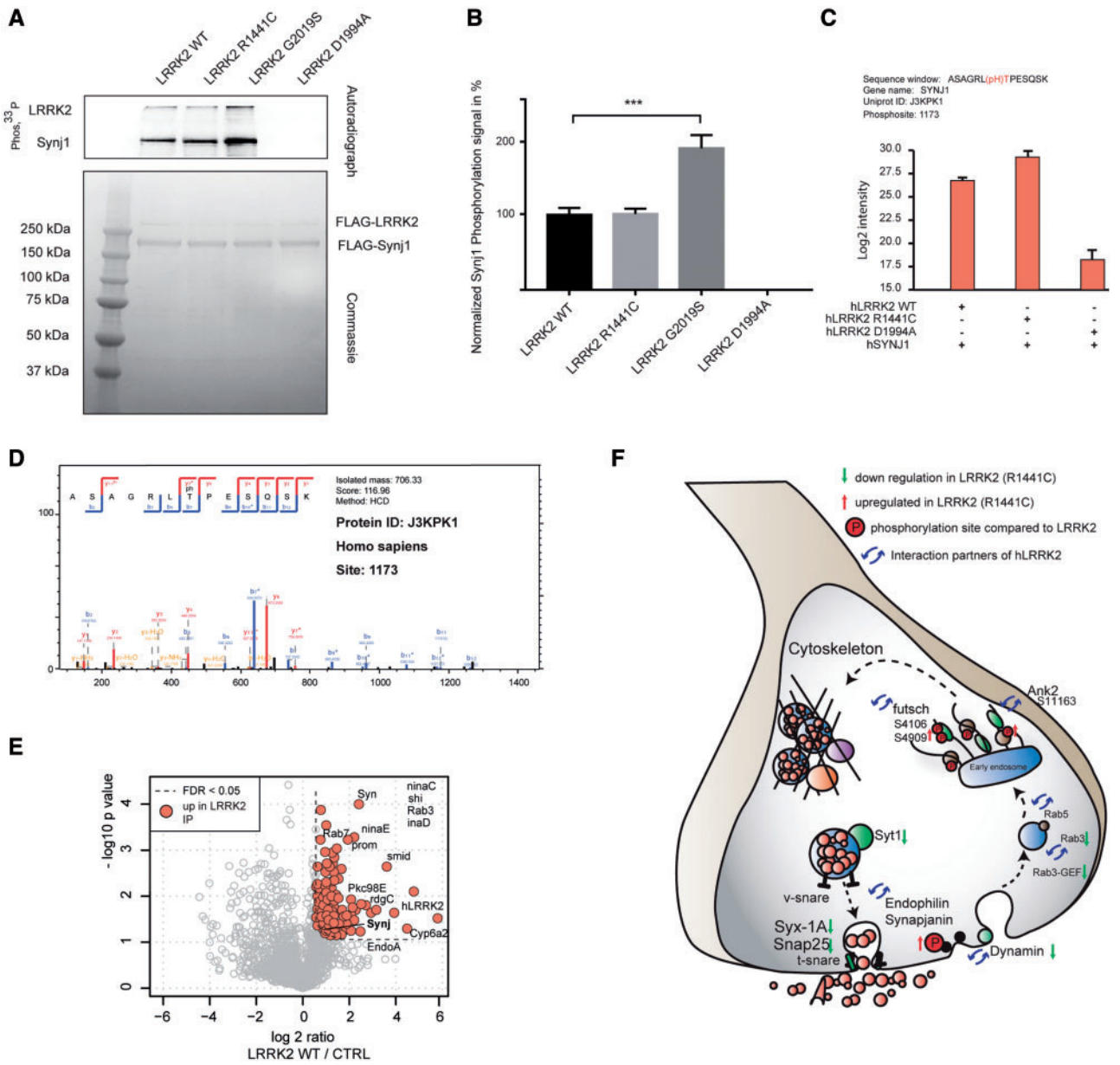

Figure 6. hLRRK2 phosphorylates Synaptojanin-1. (**A**) Human synaptojanin-1 phosphorylation by full-length human LRRK2 (WT, R1441C, G2019S and D1994A) by *in vitro* kinase assay with [^{33}P]-γ-ATP. Indicated are autoradiographs and Coomassie-stained SDS-PAGE gels to indicate equivalent protein loading. (**B**) Quantification ($n = 3$) of synaptojanin-1 phosphorylation signal normalized to total synaptojanin-1 levels. Bars indicate mean ± SEM. ***$P < 0.0001$ by one-way ANOVA with Dunnett's multiple comparison test. (**C**) GST-tagged hLRRK2 (residues 970-2527; WT, R1441C or D1994A) recombinant proteins were incubated separately with human SYNJ1 for 60 min using cold ATP. Mixtures were subjected to MS analysis to identify phospho-sites and phosphorylation of synaptojanin-1 at T1173 (Uniprot: J3KPK1) was found to be increased by LRRK2 (WT and R1441C) relative to D1994A LRRK2. (**D**) MS/MS spectra for the identified phosphorylated peptide of human synaptojanin-1 at T1173 which correlates to pT1131 in *Drosophila melanogaster*. (**E**) Interactive proteomics for hLRRK2 in *Drosophila* brain. hLRRK2 was immunoprecipitated from the fly brain using anti-FLAG antibody and subjected to LC-MS/MS analysis. Logarithmic protein ratios (hLRRK2/control flies) from two biological replicates were plotted against the -log10 *p* value from a two-sided *t*-test. FDR cutoff was set to 0.05 and missing quantitative data were replaced by a downshifted Gaussian distribution to mimic the detection limit of the mass spectrometer. (**F**) A model of how synaptic vesicle trafficking is altered by human LRRK2 expression in the *Drosophila* brain.

rodent brain (51). Primary fibroblasts from PD subjects harbouring the G2019S mutation exhibit impaired mitochondrial function and reduced intracellular ATP levels (50). Furthermore, abnormal mitochondria have been reported in the brains of aged R1441C and G2019S LRRK2 transgenic and knockin mice (68,69). A fraction of LRRK2 is also localized at synaptosomes and plays an important role in synaptic vesicle endocytosis (25,51,70,71). The formation and recycling of synaptic vesicles is an energy demanding process and reduced mitochondrial activity may have an impact on the formation of synaptic vesicles (72). Although we identify widespread changes in the abundance of general mitochondrial proteins in the tested fly strains (Fig. 4A), we observe an elevated expression of 6 mitochondrial ATP synthases associated proteins exclusively in R1441C hLRRK2 flies. This most likely suggests a dysregulation of mitochondrial activity and it is tempting to speculate that ATP-dependent synaptic vesicle formation is also affected in R1441C hLRRK2 flies. The bioinformatic analysis of WT and R1441C

hLRRK2 transgenic fly strains clearly reveals that both strains mediate neurotoxicity through different but also common pathways. For example, we observed changes in several proteins involved in synaptic vesicle exo- and endocytosis restricted to R1441C hLRRK2 flies, whereas WT hLRRK2 flies reveal no changes of SNAP25 and Rab3 at day 30. Therefore, the pathobiological mechanisms in both fly models during the course of neurodegeneration is clearly different and our analysis provides a comprehensive and quantitative dataset to further investigate the consequences of increased levels of hLRRK2 during phenotype progression in neuronal tissues of living flies.

Global phosphoproteome analysis identifies synaptojanin-1 as a novel R1441C hLRRK2 target in *Drosophila*

To provide insight into LRRK2 function and its potential kinase substrates, we performed a global phosphoproteome analysis of aged flies expressing WT and R1441C hLRRK2 (73,74). Since LRRK2 is predominantly associated with intracellular membranes and vesicular structures, the neurotoxic effects of mutant LRRK2 are most likely due to abnormal vesicular/organelle trafficking and neurotransmission. Consistent with such a notion, the overexpression of R1441G LRRK2 in transgenic mice results in disturbed dopaminergic neurotransmission (75), whereas R1441C LRRK2 transgenic mice exhibit autophagic abnormalities (68). The identification of LRRK2 kinase substrates under physiological conditions in cells or tissues is limited and a consensus phosphorylation motif based on a peptide library exists only for G2019S LRRK2 (76). Here, we identify two microtubule (MT)-associated proteins, futsch (mammalian ortholog: microtubule-associated proteins, MAPs) and Ank2, with increased phosphorylation levels in R1441C hLRRK2 flies compared to all other fly strains. The MT network plays an important role in the synaptic vesicle transport and maintenance of synaptic transmission and hence disruption of MT dynamics in neuronal axons and synapses often cause neurological diseases (77). Consistently, we also identify futsch and Ank2 in our hLRRK2 interactome study, suggesting that both MAPs are direct hLRRK2 interaction partners and most likely direct targets of LRRK2 kinase activity. Therefore, the enhanced kinase activity of R1441C hLRRK2 may induce the hyperphosphorylation of MAPs thereby altering their binding to microtubules. Futsch and Ank2 are responsible for the formation of early endosomes, correct assembly of the synaptic reserve pool, and neurotransmitter release within presynaptic active zones (78). Whether the increased phosphorylation of futsch impedes intact microtubule structures and changes the dynamics of synaptic vesicle formation or transport remains to be determined.

Depolarization of synapses causes a rapid influx of calcium that initiates synaptic vesicle exocytosis near the presynaptic plasma membrane. Synaptic vesicle docking is mediated by a complex consisting of synaptobrevin (VAMP), synaptotagmin, Rab3 and two components of the presynaptic plasma membrane, SNAP25 and syntaxin. Our study reveals a robust down-regulation of this protein complex, but no changes of the corresponding phosphopeptides. A recent study reported a similar mass spectrometry-based phosphopeptide screen of cultured fibroblasts derived from G2019S LRRK2 knockin and control mice, and identified the LRRK2-dependent phosphorylation of several Rab GTPase proteins (i.e. Rab8a, Rab10 and Rab12), some of which could also be confirmed in brain tissue (14). Although we could identify and quantify the phosphorylation of a number of Rab proteins in the fly brain, including 17 phosphorylation sites on Rab3, Rab5, Rab6, Rab7, Rab26, Rab30 and Rab35, none of these phosphorylation sites are significantly regulated by overexpressing WT and R1441C hLRRK2 relative to control flies. Moreover, we were not able to detect Rab8a, Rab10 or Rab12 phosphorylation using protein extracts from intact *Drosophila* brains in our study, as reported by Steger and colleagues in mouse fibroblasts (14). Therefore, it is possible that LRRK2-dependent Rab phosphorylation in the fly brain is either 1) rather weak and below the limit of detection of our mass spectrometric analysis, 2) that certain Rab proteins preferred by LRRK2 for phosphorylation are not sufficiently abundant within the fly brain or dopaminergic neurons (i.e. Rab8a, Rab10 or Rab12) and/or 3) that Rab proteins are not robust substrates of human LRRK2 within the context of a fly brain or dopaminergic neurons (relative to Rab phosphorylation in mouse tissues). However, we did find a significant down-regulation of Rab3 and Rab3-GEF proteins in R1441C hLRRK2 flies compared to WT hLRRK2 and control flies. This might result from dysregulated phosphorylation and suggests a direct interaction of Rab3 and LRRK2. In addition, we confirmed the LRRK2-Rab3 interaction with our protein–protein interaction analysis (Fig. 6E). Since LRRK2 phosphorylates only a subset of Rab proteins, it might be helpful in future studies to screen recombinant *Drosophila* Rab proteins to identify LRRK2-dependent phosphorylation sites and preferences.

The R1441C mutation within the Roc domain of LRRK2 is reported by some studies to increase kinase activity *in vitro* and may also induce neuronal toxicity in mammalian cells (71,74,79–81). Importantly, the R1441C mutation increases the LRRK2-dependent phosphorylation of certain Rab proteins in mammalian cells confirming that it can increase LRRK2 kinase activity given the appropriate cellular context or substrate (14). In this context, it is possible that increased levels of R1441C LRRK2 in dopaminergic neurons of the fly brain causes a dysregulation of synaptic proteins and suppression of synaptic vesicle trafficking. Previous studies indicate the direct association of LRRK2 with endosomal and autophagy pathways whereby R1441C LRRK2 induces the accumulation of autophagic vesicles (26,68,71,82–84). Further studies investigating the activation or inhibition of autophagic flux in our LRRK2 fly model may help to understand altered protein dynamics during the development of PD-related phenotypes.

One previous example of an endogenous synaptic protein target of LRRK2 is EndoA, an important regulator of synaptic vesicle endocytosis. LRRK2-dependent phosphorylation of EndoA regulates its association with membranes and facilitates synaptic vesicle endocytosis at *Drosophila* neuromuscular junctions (29). Although we observe a modest down-regulation of EndoA protein in R1441C hLRRK2 flies compared to WT hLRRK2 flies, we did not detect any phosphorylation sites on EndoA in the fly brain by our mass spectrometric approach. Instead, we identify the enhanced phosphorylation of two highly conserved sites (pT1131 and pS1142) on synaptojanin-1, a key interaction partner of EndoA (85). Synaptojanin-1 converts phosphatidylinositol-4,5-bisphosphate to phosphatidylinositol via its dual phosphatase activity and synaptojanin-1 initiates clathrin uncoating, down-regulation of actin polymerization and modulation of dynamin activity during endocytosis. The interaction between EndoA and synaptojanin-1 is critical for vesicle recycling and is mediated by the EndoA-SH3 domain and the C-terminal proline-rich domain (PRD) on synaptojanin-1. The identification of two R1441C hLRRK2-dependent phosphorylation sites (pT1131 and pS1142)

on synaptojanin-1 could potentially serve to modulate the interaction with EndoA in the fly and mammalian brain. However, the proline-rich 19-mer motif at the C-terminus of synaptojanin-1, which is responsible for interaction with the mammalian EndoA-SH3 domain is not conserved. Consistently, we detect both synjaptojanin-1 and EndoA as interaction partners of hLRRK2 and our *in vitro* kinase assays with LRRK2 and synaptojanin-1 confirms the direct phosphorylation at pT1173 within the C-terminus of human synaptojanin-1. In future, it will be important to clarify whether the hLRRK2-dependent phosphorylation of synaptojanin-1 modulates the interaction with EndoA and accordingly clathrin-dependent endocytosis. Alternatively, synaptojanin-1 is a highly dynamic protein and reversible phosphorylation could regulate its transient recruitment to synaptic vesicle membranes. Our findings indicate that R1441C hLRRK2 enhances synaptojanin-1 phosphorylation, at least within the fly brain, that could potentially be important for regulating EndoA-dependent synaptic vesicle formation under normal conditions and in PD.

Taken together, our mass spectrometric study provides a comprehensive quantitative dataset of our new human LRRK2 *Drosophila* PD models. Our phosphoproteomic analysis of R1441C hLRRK2 transgenic flies reveals novel potential hLRRK2 substrates, including several synaptic vesicle proteins such as synaptojanin-1 with increased phosphorylation. The identification of specific R1441C hLRRK2-dependent substrate phosphorylation sites will provide important insight into which molecular pathways are activated in R1441C hLRRK2 flies and we hope that our analysis will aid in the discovery of novel relevant targets for the development of new therapeutic agents to treat PD.

Materials and Methods

Drosophila stocks and harvesting

The cDNA of LRRK2 and its mutant (R1441C) were cloned into N-terminal FLAG-tagged pPFW vector (Bloomington Drosophila Center) using Gateway technology. The vectors pDEST and pDONR were used for cloning (Invitrogen). Clones containing the insert were identified by DNA restriction digest and sequencing. The plasmids were sequenced by forward primer UASP 5' GGCAAGGGTCGAGTCGATAG '3 and reverse primer K10 5'TGGTGCTATGTTTATGGCGC 3'. Plasmid DNA was microinjected into w^{1118} embryos (Vanedis Injection Services, Oslo, Norway). To obtain the *ddc::gal4*/UAS::LRRK2 fly strain *ddc::gal4* females were crossed with UAS:LRRK2 males. All fly strains were maintained with the standard cornmeal medium at 25 °C. Western blot analyses were performed to verify the hLRRK2 expression level by using an anti-FLAG antiserum. For SILAC labelling, w^{1118} flies were raised under standard conditions at 25 °C with 50–75% humidity. The SILAC food diet containing the $^{13}C_6$ lysine (Lys6)-labelled amino acid was purchased from (Silantes GmbH). Completely labelled flies were obtained from the F1 generation onwards.

Optical neutralization technique

Adult flies were mounted on microscope slides using clear nail varnish and kept under a light microscope to observe rhabdomeres as described in (86). The mean number of rhabdomere per ommatidium was calculated and rhabdomeres were counted by using cohorts of six flies. Each genotype was examined weekly during the whole life span of flies.

Survival curves

50 flies from each genotype were chosen to monitor survival rates. Flies were grown on standard media at 25 °C and fresh food media were changed every 3–4 days. To achieve survival curves, mortality was scored daily and analysed by using Kaplan-Meier survival curves. The experiment was repeated two times.

Climbing assay

Cohorts of 60 flies from each genotype were taken from 1 week to 14 weeks. The age-matched tested flies were selected randomly, anaesthetized and followed by placing in a vertical glass column (length 30 cm, diameter 1.5 cm) as described previously (87). After 60 min recovery from anaesthesia, flies were gently tapped to the bottom of the column and the number of flies that could climb to or above the midpoint (15 cm) of the cylinder in 10 s was counted and calculated as a percentage. The climbing assay was repeated three times every week.

Sample preparation and mass spectrometric analysis

The in-solution digestion protocol was performed as described previously (88). Briefly, isolated fly heads were homogenized and lysed with a buffer containing 4% SDS, 100 mM Tris-HCl, pH = 7.6. After centrifugation for 10 min, the supernatant was collected and protein concentration was measured by Bradford assay. Next, 5 μg protein extracts from each genotype (control, WT LRRK2 or R1441C LRRK2) were mixed equally with Lys6-labelled protein extracts from SILAC fly heads. The protein mixtures were precipitated with 4 volumes of ice-cold acetone at −20 °C for 4 h. Samples were centrifuged at 4 °C for 10 min, the pellet was washed with ice-cold 80% acetone, and reconstitued in 6 M Urea and 2 M Thio-Urea (in 10 mM HEPES buffer, pH = 7.5). Proteins were reduced with 10 mM dithiotreitol (DTT) for 30 min at room temperature followed by alkylation with 55 mM iodoacetamide (IAA) for 20 min in the dark. Protein digestion was performed with LysC (enzyme:substrate ratio of 1:100) (Wako) at room temperature for 3 h followed by an additional overnight digestion with LysC. The digestion was stopped by acidification (1% trifluroacetic acid in 5% acetonitrile) and the mixture was desalted on reversed phase C18 StageTips prior to mass spectrometry analysis.

Sample preparation for phosphoproteome analysis

For phosphopeptide enrichment experiments, ∼2–3 mg protein was used from each LRRK2 genotype and mixed equally with labelled protein extracts from the SILAC fly. The protein mixtures were precipitated and the protein pellets were reconstituted in 6 M Urea, 2 M Thiourea, 10 mM HEPES pH = 7.5, and subjected to in-solution digestion as described before. The peptide mixture was desalted using C18 cartridges (Waters) and the eluate was acidified with trifluoroacitic acid (TFA). Then the peptide mixture was loaded on ResourceS 1ml SCX column using an Äkta Purifier (GE Heathcare). A binary buffer system, consisting of solvent A (7 mM KH_2PO_4, 30% ACN, pH = 2.65) and solvent B (7 mM KH_2PO_4, 350 mM KCI, 30% ACN, pH = 2.65), was used to apply a gradient with increasing salt concentration over 60 min. In total, 6 fractions were collected conducting the UV 280 nm signal including flow-through from each sample that were concentrated in a speed vac. Fractions were adjusted for binding conditions of phosphopeptides to Titanium dioxide beads (TiO_2)

in 80% Acetonitrile, 6% TFA. Appropriate amounts (1:3 protein to TiO_2 beads) of TiO_2 beads (SLSC Science) were added to the peptide mixtures and incubated on a rotating wheel for 30 min. The procedure was repeated three times for flow-through and two times for fractions. Titanium dioxide beads were pooled and washed once with binding buffer (80% ACN/6% TFA). Then the TiO_2 beads were loaded on tips containing C8 material, washed twice with binding buffer and two times with washing buffer (80% ACN/3% TFA). Phosphopeptide-elution was performed by adding 3 × 25 µl of 40% Ammonia (pH=11.6) / Acetonitrile. Finally, the eluted phosphopeptides were concentrated to 2 µl and reconstituted in 10 µl 0.1% formic acid (FA)/ H_2O for mass spectrometric analysis. Note that for the analysis of phosphorylation data, first the direct ratio was calculated and then processed accordingly.

LC-MS/MS analysis

The Liquid Chromatography tandem mass spectrometry (LC-MS/MS) equipment consisted of an EASY nano-LC 1000 coupled to a nano-spray electroionization source (ESI) and a quadrupole Orbitrap mass spectrometer QExactive (Thermo Scientific). Peptides were separated on an in-house packed 50 cm column (1.9 µm C18 beads) using a binary buffer system: A) 0.1% formic acid and B) 0.1% formic acid in 80% acetonitrile. The content of buffer B was raised from 10 to 38% within 210 min and followed by an increase to 60% within 10 min. Followed by a washing step of 95% B for 10 min and a re-equilibration at 5% B for 10 min. Eluting peptides were ionized by an applied voltage of approx. 2.0 kV. The capillary temperature was 275 °C and the S-lens RF level was set to 64. MS1 spectra were acquired using a resolution of 70,000 (at 200 m/z), an Automatic Gain Control (AGC) target of 3e6, and a maximum injection time of 20 ms in a scan range of 300–1750 Th. In a data dependent mode, the 10 most intense peaks were selected for isolation and fragmentation in the HCD cell using a normalized collision energy of 25. Dynamic exclusion was enabled and set to 25 s. The MS/MS scan properties were: 17.500 resolution at 200 m/z, an isolation window of 2.1 Th, an AGC target of 5e5 and a maximum injection time of 60 ms. The gradient and settings for MS/MS scan properties were different for phosphoproteome experiments: Gradient time was 150 min and the MS/MS scan resolution was 35.000 (200 m/z), max. injection time was 120 ms aiming for an AGC target of 5e5, and an isolation window of 1.8 Th was used. In vitro kinase assay was measured with similar settings but a gradient time of 60 min was applied. Immunoprecipitation experiments were performed with an LTQ-Orbitrap Velos mass spectrometer (Thermo Fisher) as described elsewhere (89).

Raw data processing

The mass spectrometric raw data were analysed by the MaxQuant software package (version 1.4.7.2) (90). Proteins were identified using the implemented Andromeda search engine and *D.melanogaster* (flybase, release 5.13, Indiana University, IN, USA) database with common contaminants. Oxidation of methionine and acetylation of the protein N-terminus were selected as variable modifications and carbamidomethylation of cysteines were set as a fixed modification. LysC was selected as the protease and a maximum of 2 missed cleavages were allowed. A mass tolerances of 0.5 Da was selected for fragment ions and only peptides with a minimum of six amino acids were considered for identification. The false discovery rate was set to 1% on the peptide-spectrum-match and protein level using the implemented decoy algorithm. The minimum ratio count was set to 2. Data analysis and visualization were done by using Perseus software (Max Plank Institute, Martinsried) and the statistical environment R. Gene Ontology annotation (based on Uniprot identifiers) was carried out by Perseus. Significant differentially expressed proteins within the LRRK2 dataset including WT hLRRK2, R1441C hLRRK2 and control flies were identified by a permutation-based FDR approach using a cutoff of 0.01, fudge factor s0 = 0.3 and 500 permutations. Significant differentially expressed phosphopeptides were identified by using a one-sided *t*-test and a cutoff, if not stated differently, of log2 fold change > 0.58 and *P* value < 0.05 was used. 1D enrichment, GO, KEEG and GESA annotation and principal component analysis were performed in Perseus software (MPI, Martinsried) using default settings.

Immunoprecipitation

The heads from *ddc*-Gal4 control and hLRRK2-overexpressing flies were homogenized in modified RIPA lysis buffer (50 mM Tris-HCl pH 7.5, 150 mM NaCl, 1% NP-40, 1 mM EDTA, 0.1% Natriumdeoxycholate). After centrifugation at 16,000*g* for 10 min the clear supernatant was removed and incubated with anti-FLAG antiserum coated beads (M2 FLAG, Sigma Aldrich) for 3 h with rotation at 4 °C. Beads were then washed twice with the modified RIPA buffer. Proteins were eluted from the beads by adding 4x LDS loading buffer and 1 µl DDT, followed by boiling for 5 min at 95 °C. Samples were separated by SDS-PAGE (4–12% Bis-Tris gels. Invitrogen) and in-gel protein digestion was performed as described previously (91).

Western blot analysis

Adult fly heads were homogenized in 4% SDS, 0.1 M Tris-HCl, pH 7.5. After the Bradford protein assay, equal protein amounts were resolved by SDS-PAGE (4–12% Bis-Tris gels). Proteins were transferred onto nitrocellulose membranes (Milipore) and the membrane was blocked with TBST containing 5% milk. Membranes were incubated with anti-FLAG antibody (1:1000, Sigma), and rabbit anti-Tan antibody (ap63, 1:2500) (92). Protein detection was performed using enhanced chemiluminescence (Pierce) in a ChemiDoc (Biorad) instrument.

Immunofluorescence

Heads from from 4 week-old flies were fixed with 4% paraformaldehyde in 0.1 M phosphate buffer pH 7.4 for 3 h at 4 °C. The fixative was replaced by 25% sucrose in Ringeŕs solution and flies were incubated overnight at 4 °C. Heads were embedded in Tissue-Tek (Sakura Fintek, Zoeterwoude, The Netherlands) and frozen in liquid nitrogen. Sections were made using a Leica HM 5030 Cryostat. Probes were washed twice for 10 mins with TBST and blocked with 1% normal goat serum (NGS) in TBST for 30 mins (all at RT). Primary antibodies were applied at 4 °C overnight at the following dilution: rabbit anti-Tan (ap63, 1:20,000) and mouse anti-NC82 (1:10, DSHB, Iowa, United States). Slides were incubated at RT for 30 mins, washed twice for 10 mins with TBST and incubated with secondary antibodies at 1:400 in TBST/1% NGS (Alexa488-conjugated goat anti-rabbit or Alexa594-conjugated goat anti-mouse, Molecular Probes) overnight at 4 °C. After washing twice for 10 min at RT using TBST, slices were mounted in DakoCytomation Glycergel

(DakoCytomation, Hamburg, Germany) and fluorescence signals were imaged using a Leica TCS SP2 confocal microscope. In order to obtain comparable results all procedure was done simultaneously using antibodies and control genotypes.

For whole mount staining, brains were dissected and fixed within 4% PFA for 45 min on ice. After fixation brains were washed 6 × 20 min with PBST at RT and incubated with washing buffer + 4% NGS for 3 h. Then, brains were incubated with an anti-TH antibody (1:1000, Abcam) at 4 °C over night. After washing 6 × 20 min at RT the secondary antibody (Alexa488) was added over night at 4 °C. Brains were washed 6 x 20 min at RT and mounted in Vectashield mounting medium + DAPI.

In vitro kinase assay

In total, 300 ng of purified recombinant human synaptojanin-1 (Origene) was incubated with 1 nM recombinant GST-tagged human LRRK2 (970-2527; WT, R1441C or D1994A; Invitrogen) in 5 µl 10x kinase buffer (Cell Signalling Technology), 1 µl [γ-^{33}P]-ATP (1 µCi) in a final volume of 15 µl without incubation and incubated for 60 mins at 30 °C or quenched directly. Where indicated, an increasing concentration of LRRK2-IN-1 (0.075, 0.3, 0.5 or 1 µM) was added to the samples and incubated for 60 mins. The reaction mixtures were terminated by adding 5 µl of 4x LDS sample buffer (Invitrogen) followed by denaturing the samples at 96 °C for 10 mins. As a control, we used either synaptojanin-1 or LRRK2 along with all other components. Each sample was loaded in 10 well 4–12% Bis-tris SDS-PAGE gels (Invitrogen) and run at 160 volt for 2 h. Autoradiography was detected from the dried gels using X-ray film. Identical assay conditions were used for synaptojanin-1 phospho-site detection by mass spectrometry. A 60 min LC-MS/MS gradient was applied after in-solution trypsin digestion and desalting by StageTip technique. Identification of phosphorylation sites was performed by MaxQuant using default settings and the human Uniprot reference proteome (11.2014 downloaded). The minimal score for modified peptides was set to 0. The *in vitro* phosphorylation of human synaptojanin-1 by full-length human LRRK2 was performed using [γ-^{33}P]-ATP and immunopurified soluble 1xFLAG-/GFP-tagged synaptojanin-1 and 3xFLAG-tagged LRRK2 (WT, R1441C, G2019S or D1994A) derived from HEK-293T cells by anti-FLAG-M2-sepharose (Sigma Aldrich) with elution using either 1xFLAG or 3xFLAG peptide (Sigma Aldrich) and quantitation by BCA assay (Perbio). Samples were resolved by SDS-PAGE and either transferred to PVDF membranes for detection by autoradiography, or stained with Coomassie colloidal blue (G250, Biorad) to assess protein levels and purity. The FLAG-/GFP-tagged human synaptojanin-1 (145 kDa isoform) expression plasmid was a kind gift from Pietro De Camilli (Addgene plasmid # 22293), whereas FLAG-tagged human LRRK2 (WT, R1441C, G2019S and D1994A) expression plasmids have been reported previously (26,28).

Supplementary Material

Supplementary Material is available at *HMG* online.

Acknowledgements

We thank Sylvia Jeratsch for excellent technical assistance. The authors thank Milka Uhlirova for Drosophila stock maintenance.

Conflict of Interest statement. None declared.

Funding

This work was supported by the DFG (Excellence Cluster Cardio-Pulmonary System), the LOEWE Center for Cell and Gene Therapy, the German Center for Cardiovascular Research, the Universities of Giessen and Marburg Lung Center, the National Institutes of Health (R01 NS091719 to DJM) and the Swiss National Science Foundation (Grant No. 31003A_144063 to DJM). SI was the recipient of an ESR fellowship receiving funding for this project by the European Community's Framework Programme (FP7) under grant agreement number TRANSPOL – 264399. WJ initiated this project while he was the recipient of an ITN-fellowship INTCHEM.

References

1. Lees, A.J., Hardy, J. and Revesz, T. (2009) Parkinson's disease. *Lancet*, **373**, 2055–2066.
2. Gasser, T. (2009) Molecular pathogenesis of Parkinson disease: insights from genetic studies. *Expert Rev. Mol. Med.*, **11**, e22.
3. Mata, I.F., Wedemeyer, W.J., Farrer, M.J., Taylor, J.P. and Gallo, K.A. (2006) LRRK2 in Parkinson's disease: protein domains and functional insights. *Trends Neurosci.*, **29**, 286–293.
4. Bonifati, V. (2014) Genetics of Parkinson's disease–state of the art, 2013. *Parkinsonism Relat. Disord.*, **20**, S23–S28.
5. Zimprich, A., Biskup, S., Leitner, P., Lichtner, P., Farrer, M., Lincoln, S., Kachergus, J., Hulihan, M., Uitti, R.J., Calne, D.B., *et al.* (2004) Mutations in LRRK2 cause autosomal-dominant parkinsonism with pleomorphic pathology. *Neuron*, **44**, 601–607.
6. Paisan-Ruiz, C., Jain, S., Evans, E.W., Gilks, W.P., Simon, J., van der Brug, M., Lopez de Munain, A., Aparicio, S., Gil, A.M., Khan, N., *et al.* (2004) Cloning of the gene containing mutations that cause PARK8-linked Parkinson's disease. *Neuron*, **44**, 595–600.
7. Biskup, S. and West, A.B. (2009) Zeroing in on LRRK2-linked pathogenic mechanisms in Parkinson's disease. *Biochim. Biophys. Acta*, **1792**, 625–633.
8. Simon-Sanchez, J., Schulte, C., Bras, J.M., Sharma, M., Gibbs, J.R., Berg, D., Paisan-Ruiz, C., Lichtner, P., Scholz, S.W., Hernandez, D.G., *et al.* (2009) Genome-wide association study reveals genetic risk underlying Parkinson's disease. *Nat. Genet.*, **41**, 1308–1312.
9. Mata, I.F., Hutter, C.M., Gonzalez-Fernandez, M.C., de Pancorbo, M.M., Lezcano, E., Huerta, C., Blazquez, M., Ribacoba, R., Guisasola, L.M., Salvador, C., *et al.* (2009) Lrrk2 R1441G-related Parkinson's disease: evidence of a common founding event in the seventh century in Northern Spain. *Neurogenetics*, **10**, 347–353.
10. Zabetian, C.P., Yamamoto, M., Lopez, A.N., Ujike, H., Mata, I.F., Izumi, Y., Kaji, R., Maruyama, H., Morino, H., Oda, M., *et al.* (2009) LRRK2 mutations and risk variants in Japanese patients with Parkinson's disease. *Mov. Disord.*, **24**, 1034–1041.
11. Kachergus, J., Mata, I.F., Hulihan, M., Taylor, J.P., Lincoln, S., Aasly, J., Gibson, J.M., Ross, O.A., Lynch, T., Wiley, J., *et al.* (2005) Identification of a novel LRRK2 mutation linked to autosomal dominant parkinsonism: evidence of a common founder across European populations. *Am. J. Hum. Genet.*, **76**, 672–680.
12. Gloeckner, C.J., Kinkl, N., Schumacher, A., Braun, R.J., O'Neill, E., Meitinger, T., Kolch, W., Prokisch, H. and Ueffing, M. (2006) The Parkinson disease causing LRRK2 mutation I2020T is associated with increased kinase activity. *Hum. Mol. Genet.*, **15**, 223–232.

13. Gloeckner, C.J., Schumacher, A., Boldt, K. and Ueffing, M. (2009) The Parkinson disease-associated protein kinase LRRK2 exhibits MAPKKK activity and phosphorylates MKK3/6 and MKK4/7, in vitro. *J. Neurochem.*, **109**, 959–968.
14. Steger, M., Tonelli, F., Ito, G., Davies, P., Trost, M., Vetter, M., Wachter, S., Lorentzen, E., Duddy, G., Wilson, S., *et al.* (2016) Phosphoproteomics reveals that Parkinson's disease kinase LRRK2 regulates a subset of Rab GTPases. *Elife*, **5**, e12813.
15. Liao, J., Wu, C.X., Burlak, C., Zhang, S., Sahm, H., Wang, M., Zhang, Z.Y., Vogel, K.W., Federici, M., Riddle, S.M., *et al.* (2014) Parkinson disease-associated mutation R1441H in LRRK2 prolongs the "active state" of its GTPase domain. *Proc. Natl Acad. Sci. U S A*, **111**, 4055–4060.
16. Li, X., Tan, Y.C., Poulose, S., Olanow, C.W., Huang, X.Y. and Yue, Z. (2007) Leucine-rich repeat kinase 2 (LRRK2)/PARK8 possesses GTPase activity that is altered in familial Parkinson's disease R1441C/G mutants. *J. Neurochem.*, **103**, *238–247*,
17. Guo, L., Gandhi, P.N., Wang, W., Petersen, R.B., Wilson-Delfosse, A.L. and Chen, S.G. (2007) The Parkinson's disease-associated protein, leucine-rich repeat kinase 2 (LRRK2), is an authentic GTPase that stimulates kinase activity. *Exp. Cell Res.*, **313**, 3658–3670.
18. Greggio, E., Jain, S., Kingsbury, A., Bandopadhyay, R., Lewis, P., Kaganovich, A., van der Brug, M.P., Beilina, A., Blackinton, J., Thomas, K.J., *et al.* (2006) Kinase activity is required for the toxic effects of mutant LRRK2/dardarin. *Neurobiol. Dis.*, **23**, 329–341.
19. Wang, D., Tang, B., Zhao, G., Pan, Q., Xia, K., Bodmer, R. and Zhang, Z. (2008) Dispensable role of Drosophila ortholog of LRRK2 kinase activity in survival of dopaminergic neurons. *Mol. Neurodegener.*, **3**, 3.
20. Bosgraaf, L. and Van Haastert, P.J. (2003) Roc, a Ras/GTPase domain in complex proteins. *Biochim. Biophys. Acta*, **1643**, 5–10.
21. Jaleel, M., Nichols, R.J., Deak, M., Campbell, D.G., Gillardon, F., Knebel, A. and Alessi, D.R. (2007) LRRK2 phosphorylates moesin at threonine-558: characterization of how Parkinson's disease mutants affect kinase activity. *Biochem. J.*, **405**, 307–317.
22. Gillardon, F. (2009) Leucine-rich repeat kinase 2 phosphorylates brain tubulin-beta isoforms and modulates microtubule stability–a point of convergence in parkinsonian neurodegeneration?. *J. Neurochem.*, **110**, 1514–1522.
23. Dusonchet, J., Li, H., Guillily, M., Liu, M., Stafa, K., Derada Troletti, C., Boon, J.Y., Saha, S., Glauser, L., Mamais, A., *et al.* (2014) A Parkinson's disease gene regulatory network identifies the signaling protein RGS2 as a modulator of LRRK2 activity and neuronal toxicity. *Hum. Mol. Genet.*, **23**, 4887–4905.
24. Martin, I., Kim, J.W., Lee, B.D., Kang, H.C., Xu, J.C., Jia, H., Stankowski, J., Kim, M.S., Zhong, J., Kumar, M., *et al.* (2014) Ribosomal protein s15 phosphorylation mediates LRRK2 neurodegeneration in Parkinson's disease. *Cell*, **157**, 472–485.
25. Shin, N., Jeong, H., Kwon, J., Heo, H.Y., Kwon, J.J., Yun, H.J., Kim, C.H., Han, B.S., Tong, Y., Shen, J., *et al.* (2008) LRRK2 regulates synaptic vesicle endocytosis. *Exp. Cell Res.*, **314**, 2055–2065.
26. Stafa, K., Tsika, E., Moser, R., Musso, A., Glauser, L., Jones, A., Biskup, S., Xiong, Y., Bandopadhyay, R., Dawson, V.L., *et al.* (2014) Functional interaction of Parkinson's disease-associated LRRK2 with members of the dynamin GTPase superfamily. *Hum. Mol. Genet.*, **23**, 2055–2077.
27. Xiong, Y., Dawson, V.L.,. and Dawson, T.M. (2012) LRRK2 GTPase dysfunction in the pathogenesis of Parkinson's disease. *Biochem. Soc. Trans.*, **40**, 1074–1079.
28. Stafa, K., Trancikova, A., Webber, P.J., Glauser, L., West, A.B. and Moore, D.J. (2012) GTPase activity and neuronal toxicity of Parkinson's disease-associated LRRK2 is regulated by ArfGAP1. *PLoS Genet.*, **8**, e1002526.
29. Matta, S., Van Kolen, K., da Cunha, R., van den Bogaart, G., Mandemakers, W., Miskiewicz, K., De Bock, P.J., Morais, V.A., Vilain, S., Haddad, D., *et al.* (2012) LRRK2 controls an EndoA phosphorylation cycle in synaptic endocytosis. *Neuron.*, **75**, 1008–1021.
30. Imai, Y., Gehrke, S., Wang, H.Q., Takahashi, R., Hasegawa, K., Oota, E. and Lu, B. (2008) Phosphorylation of 4E-BP by LRRK2 affects the maintenance of dopaminergic neurons in Drosophila. *EMBO J.*, **27**, 2432–2443.
31. Yang, D., Li, T., Liu, Z., Arbez, N., Yan, J., Moran, T.H., Ross, C.A. and Smith, W.W. (2012) LRRK2 kinase activity mediates toxic interactions between genetic mutation and oxidative stress in a Drosophila model: suppression by curcumin. *Neurobiol. Dis.*, **47**, 385–392.
32. Liu, Z., Wang, X., Yu, Y., Li, X., Wang, T., Jiang, H., Ren, Q., Jiao, Y., Sawa, A., Moran, T., *et al.* (2008) A Drosophila model for LRRK2-linked parkinsonism. *Proc. Natl Acad. Sci. U S A*, **105**, 2693–2698.
33. Lee, S., Liu, H.P., Lin, W.Y., Guo, H. and Lu, B. (2010) LRRK2 kinase regulates synaptic morphology through distinct substrates at the presynaptic and postsynaptic compartments of the Drosophila neuromuscular junction. *J. Neurosci.*, **30**, 16959–16969.
34. Laverty, C., Li, F., Belikoff, E.J. and Scott, M.J. (2011) Abnormal dosage compensation of reporter genes driven by the Drosophila glass multiple reporter (GMR) enhancer-promoter. *PLoS One*, **6**, e20455.
35. Feany, M.B. and Bender, W.W. (2000) A Drosophila model of Parkinson's disease. *Nature*, **404**, 394–398.
36. Mao, Z. and Davis, R.L. (2009) Eight different types of dopaminergic neurons innervate the Drosophila mushroom body neuropil: anatomical and physiological heterogeneity. *Front. Neural. Circuits*, **3**, 5.
37. Sury, M.D., Chen, J.X. and Selbach, M. (2014) In vivo stable isotope labeling by amino acids in Drosophila melanogaster. *Methods Mol. Biol.*, **1188**, 85–93.
38. Liu, E.W., Wang, S.J., Liu, Y., Liu, W., Chen, Z.S., Li, X.Y., A, L.Y. and Wu, Z.Y. (2011) [Mortality of HIV infected clients treated with methadone maintenance treatment in Yili Kazakh autonomous prefecture]. *Zhonghua Yu Fang Yi Xue Za Zhi*, **45**, 979–984.
39. Pevsner, J., Hsu, S.C., Braun, J.E., Calakos, N., Ting, A.E., Bennett, M.K. and Scheller, R.H. (1994) Specificity and regulation of a synaptic vesicle docking complex. *Neuron*, **13**, 353–361.
40. Broadie, K., Prokop, A., Bellen, H.J., O'Kane, C.J., Schulze, K.L. and Sweeney, S.T. (1995) Syntaxin and synaptobrevin function downstream of vesicle docking in Drosophila. *Neuron*, **15**, 663–673.
41. Kidokoro, Y. (2003) Roles of SNARE proteins and synaptotagmin I in synaptic transmission: studies at the Drosophila neuromuscular synapse. *Neurosignals*, **12**, 13–30.
42. Glavan, G., Schliebs, R. and Zivin, M. (2009) Synaptotagmins in neurodegeneration. *Anat. Rec. (Hoboken)*, **292**, 1849–1862.
43. Tong, Y., Pisani, A., Martella, G., Karouani, M., Yamaguchi, H., Pothos, E.N. and Shen, J. (2009) R1441C mutation in LRRK2

impairs dopaminergic neurotransmission in mice. *Proc.. Natl Acad. Sci. U S A*, **106**, 14622–14627.
44. Mencacci, N.E., Isaias, I.U., Reich, M.M., Ganos, C., Plagnol, V., Polke, J.M., Bras, J., Hersheson, J., Stamelou, M., Pittman, A.M., *et al.* (2014) Parkinson's disease in GTP cyclohydrolase 1 mutation carriers. *Brain*, **137**, 2480–2492.
45. Blau, N., Bonafe, L. and Thony, B. (2001) Tetrahydrobiopterin deficiencies without hyperphenylalaninemia: diagnosis and genetics of dopa-responsive dystonia and sepiapterin reductase deficiency. *Mol. Genet. Metab.*, **74**, 172–185.
46. True, J.R., Yeh, S.D., Hovemann, B.T., Kemme, T., Meinertzhagen, I.A., Edwards, T.N., Liou, S.R., Han, Q.,. and Li, J. (2005) Drosophila tan encodes a novel hydrolase required in pigmentation and vision. *PLoS Genet.*, **1**, e63.
47. Parisiadou, L. and Cai, H. (2010) LRRK2 function on actin and microtubule dynamics in Parkinson disease. *Commun. Integr. Biol.*, **3**, 396–400.
48. Whitworth, A.J., Theodore, D.A., Greene, J.C., Benes, H., Wes, P.D. and Pallanck, L.J. (2005) Increased glutathione S-transferase activity rescues dopaminergic neuron loss in a Drosophila model of Parkinson's disease. *Proc. Natl Acad. Sci. U S A*, **102**, 8024–8029.
49. Winklhofer, K.F. and Haass, C. (2010) Mitochondrial dysfunction in Parkinson's disease. *Biochim. Biophys. Acta*, **1802**, 29–44.
50. Mortiboys, H., Johansen, K.K., Aasly, J.O. and Bandmann, O. (2010) Mitochondrial impairment in patients with Parkinson disease with the G2019S mutation in LRRK2. *Neurology*, **75**, 2017–2020.
51. Biskup, S., Moore, D.J., Celsi, F., Higashi, S., West, A.B., Andrabi, S.A., Kurkinen, K., Yu, S.W., Savitt, J.M., Waldvogel, H.J., *et al.* (2006) Localization of LRRK2 to membranous and vesicular structures in mammalian brain. *Ann. Neurol.*, **60**, 557–569.
52. Dason, J.S., Romero-Pozuelo, J., Atwood, H.L. and Ferrus, A. (2012) Multiple roles for frequenin/NCS-1 in synaptic function and development. *Mol. Neurobiol.*, **45**, 388–402.
53. Dihanich, S., Civiero, L., Manzoni, C., Mamais, A., Bandopadhyay, R., Greggio, E. and Lewis, P.A. (2014) GTP binding controls complex formation by the human ROCO protein MASL1. *Febs. J.*, **281**, 261–274.
54. Sato, H., Arawaka, S., Hara, S., Fukushima, S., Koga, K., Koyama, S. and Kato, T. (2011) Authentically phosphorylated alpha-synuclein at Ser129 accelerates neurodegeneration in a rat model of familial Parkinson's disease. *J. Neurosci.*, **31**, 16884–16894.
55. Chen, L. and Feany, M.B. (2005) Alpha-synuclein phosphorylation controls neurotoxicity and inclusion formation in a Drosophila model of Parkinson disease. *Nat. Neurosci.*, **8**, 657–663.
56. Mochly-Rosen, D., Das, K. and Grimes, K.V. (2012) Protein kinase C, an elusive therapeutic target?. *Nat. Rev. Drug Discov.*, **11**, 937–957.
57. Koch, I., Schwarz, H., Beuchle, D., Goellner, B., Langegger, M. and Aberle, H. (2008) Drosophila ankyrin 2 is required for synaptic stability. *Neuron*, **58**, 210–222.
58. Verstreken, P., Koh, T.W., Schulze, K.L., Zhai, R.G., Hiesinger, P.R., Zhou, Y., Mehta, S.Q., Cao, Y., Roos, J. and Bellen, H.J. (2003) Synaptojanin is recruited by endophilin to promote synaptic vesicle uncoating. *Neuron*, **40**, 733–748.
59. McPherson, P.S., Garcia, E.P., Slepnev, V.I., David, C., Zhang, X., Grabs, D., Sossin, W.S., Bauerfeind, R., Nemoto, Y. and De Camilli, P. (1996) A presynaptic inositol-5-phosphatase. *Nature*, **379**, 353–357.
60. Quadri, M., Fang, M., Picillo, M., Olgiati, S., Breedveld, G.J., Graafland, J., Wu, B., Xu, F., Erro, R., Amboni, M., *et al.* (2013) Mutation in the SYNJ1 gene associated with autosomal recessive, early-onset Parkinsonism. *Hum. Mutat.*, **34**, 1208–1215.
61. Krebs, C.E., Karkheiran, S., Powell, J.C., Cao, M., Makarov, V., Darvish, H., Di Paolo, G., Walker, R.H., Shahidi, G.A., Buxbaum, J.D., *et al.* (2013) The Sac1 domain of SYNJ1 identified mutated in a family with early-onset progressive Parkinsonism with generalized seizures. *Hum. Mutat.*, **34**, 1200–1207.
62. Dephoure, N., Zhou, C., Villen, J., Beausoleil, S.A., Bakalarski, C.E., Elledge, S.J. and Gygi, S.P. (2008) A quantitative atlas of mitotic phosphorylation. *Proc. Natl Acad. Sci. U S A*, **105**, 10762–10767.
63. Lundby, A., Secher, A., Lage, K., Nordsborg, N.B., Dmytriyev, A., Lundby, C. and Olsen, J.V. (2012) Quantitative maps of protein phosphorylation sites across 14 different rat organs and tissues. *Nat. Commun.*, **3**, 876.
64. Sen, S., Webber, P.J. and West, A.B. (2009) Dependence of leucine-rich repeat kinase 2 (LRRK2) kinase activity on dimerization. *J. Biol. Chem.*, **284**, 36346–36356.
65. Greggio, E., Taymans, J.M., Zhen, E.Y., Ryder, J., Vancraenenbroeck, R., Beilina, A., Sun, P., Deng, J., Jaffe, H., Baekelandt, V., *et al.* (2009) The Parkinson's disease kinase LRRK2 autophosphorylates its GTPase domain at multiple sites. *Biochem. Biophys. Res. Commun.*, **389**, 449–454.
66. Gloeckner, C.J., Boldt, K., von Zweydorf, F., Helm, S., Wiesent, L., Sarioglu, H. and Ueffing, M. (2010) Phosphopeptide analysis reveals two discrete clusters of phosphorylation in the N-terminus and the Roc domain of the Parkinson-disease associated protein kinase LRRK2. *J. Proteome Res.*, **9**, 1738–1745.
67. Langston, R.G., Rudenko, I.N. and Cookson, M.R. (2016) The function of orthologues of the human Parkinson's disease gene LRRK2 across species: implications for disease modelling in preclinical research. *Biochem. J.*, **473**, 221–232.
68. Ramonet, D., Daher, J.P., Lin, B.M., Stafa, K., Kim, J., Banerjee, R., Westerlund, M., Pletnikova, O., Glauser, L., Yang, L., *et al.* (2011) Dopaminergic neuronal loss, reduced neurite complexity and autophagic abnormalities in transgenic mice expressing G2019S mutant LRRK2. *PLoS One*, **6**, e18568.
69. Yue, M., Hinkle, K.M., Davies, P., Trushina, E., Fiesel, F.C., Christenson, T.A., Schroeder, A.S., Zhang, L., Bowles, E., Behrouz, B., *et al.* (2015) Progressive dopaminergic alterations and mitochondrial abnormalities in LRRK2 G2019S knock-in mice. *Neurobiol. Dis.*, **78**, 172–195.
70. Piccoli, G., Condliffe, S.B., Bauer, M., Giesert, F., Boldt, K., De Astis, S., Meixner, A., Sarioglu, H., Vogt-Weisenhorn, D.M., Wurst, W., *et al.* (2011) LRRK2 controls synaptic vesicle storage and mobilization within the recycling pool. *J. Neurosci.*, **31**, 2225–2237.
71. Xiong, Y., Coombes, C.E., Kilaru, A., Li, X., Gitler, A.D., Bowers, W.J., Dawson, V.L., Dawson, T.M. and Moore, D.J. (2010) GTPase activity plays a key role in the pathobiology of LRRK2. *PLoS Genet.*, **6**, e1000902.
72. Verstreken, P., Ly, C.V., Venken, K.J., Koh, T.W., Zhou, Y. and Bellen, H.J. (2005) Synaptic mitochondria are critical for mobilization of reserve pool vesicles at Drosophila neuromuscular junctions. *Neuron*, **47**, 365–378.
73. Ito, G., Okai, T., Fujino, G., Takeda, K., Ichijo, H., Katada, T. and Iwatsubo, T. (2007) GTP binding is essential to the protein kinase activity of LRRK2, a causative gene product for familial Parkinson's disease. *Biochemistry*, **46**, 1380–1388.

74. West, A.B., Moore, D.J., Choi, C., Andrabi, S.A., Li, X., Dikeman, D., Biskup, S., Zhang, Z., Lim, K.L., Dawson, V.L., *et al*. (2007) Parkinson's disease-associated mutations in LRRK2 link enhanced GTP-binding and kinase activities to neuronal toxicity. *Hum. Mol. Genet.*, **16**, 223–232.
75. Liu, H.F., Lu, S., Ho, P.W., Tse, H.M., Pang, S.Y., Kung, M.H., Ho, J.W., Ramsden, D.B., Zhou, Z.J.,. and Ho, S.L. (2014) LRRK2 R1441G mice are more liable to dopamine depletion and locomotor inactivity. *Ann. Clin. Transl Neurol.*, **1**, 199–208.
76. Pungaliya, P.P., Bai, Y., Lipinski, K., Anand, V.S., Sen, S., Brown, E.L., Bates, B., Reinhart, P.H., West, A.B., Hirst, W.D., *et al*. (2010) Identification and characterization of a leucine-rich repeat kinase 2 (LRRK2) consensus phosphorylation motif. *PLoS One*, **5**, e13672.
77. Trotta, N., Orso, G., Rossetto, M.G., Daga, A. and Broadie, K. (2004) The hereditary spastic paraplegia gene, spastin, regulates microtubule stability to modulate synaptic structure and function. *Curr. Biol.*, **14**, 1135–1147.
78. Lepicard, S., Franco, B., de Bock, F. and Parmentier, M.L. (2014) A presynaptic role of microtubule-associated protein 1/Futsch in Drosophila: regulation of active zone number and neurotransmitter release. *J. Neurosci.*, **34**, 6759–6771.
79. Smith, W.W., Pei, Z., Jiang, H., Dawson, V.L., Dawson, T.M. and Ross, C.A. (2006) Kinase activity of mutant LRRK2 mediates neuronal toxicity. *Nat. Neurosci.*, **9**, 1231–1233.
80. Smith, W.W., Pei, Z., Jiang, H., Moore, D.J., Liang, Y., West, A.B., Dawson, V.L., Dawson, T.M. and Ross, C.A. (2005) Leucine-rich repeat kinase 2 (LRRK2) interacts with parkin, and mutant LRRK2 induces neuronal degeneration. *Proc. Natl Acad. Sci. U S A*, **102**, 18676–18681.
81. McLeod, M., Hong, M., Mukhida, K., Sadi, D., Ulalia, R. and Mendez, I. (2006) Erythropoietin and GDNF enhance ventral mesencephalic fiber outgrowth and capillary proliferation following neural transplantation in a rodent model of Parkinson's disease. *Eur. J. Neurosci.*, **24**, 361–370.
82. Alegre-Abarrategui, J. and Wade-Martins, R. (2009) Parkinson disease, LRRK2 and the endocytic-autophagic pathway. *Autophagy*, **5**, 1208–1210.
83. Higashi, S., Moore, D.J., Yamamoto, R., Minegishi, M., Sato, K., Togo, T., Katsuse, O., Uchikado, H., Furukawa, Y., Hino, H., *et al*. (2009) Abnormal localization of leucine-rich repeat kinase 2 to the endosomal-lysosomal compartment in lewy body disease. *J. Neuropathol. Exp. Neurol.*, **68**, 994–1005.
84. Plowey, E.D., Cherra, S.J., 3rd, Liu, Y.J. and Chu, C.T. (2008) Role of autophagy in G2019S-LRRK2-associated neurite shortening in differentiated SH-SY5Y cells. *J. Neurochem.*, **105**, 1048–1056.
85. Gad, H., Ringstad, N., Low, P., Kjaerulff, O., Gustafsson, J., Wenk, M., Di Paolo, G., Nemoto, Y., Crun, J., Ellisman, M.H., *et al*. (2000) Fission and uncoating of synaptic clathrin-coated vesicles are perturbed by disruption of interactions with the SH3 domain of endophilin. *Neuron*, **27**, 301–312.
86. Xu, H., Lee, S.J., Suzuki, E., Dugan, K.D., Stoddard, A., Li, H.S., Chodosh, L.A. and Montell, C. (2004) A lysosomal tetraspanin associated with retinal degeneration identified via a genome-wide screen. *Embo J.*, **23**, 811–822.
87. Ganetzky, B. and Flanagan, J.R. (1978) On the relationship between senescence and age-related changes in two wild-type strains of Drosophila melanogaster. *Exp. Gerontol.*, **13**, 189–196.
88. Nolte, H., Hölper, S., Housley, M.P., Islam, S., Piller, T., Konzer, A., Stainier, D.Y., Braun, T. and Krüger, M. (2014) Dynamics of zebrafish fin regeneration using a pulsed silac approach. *Proteomics*, **15**, 739–751.
89. Drexler, H.C., Ruhs, A., Konzer, A., Mendler, L., Bruckskotten, M., Looso, M., Günther, S., Boettger, T., Krüger, M. and Braun, T. (2012) On marathons and Sprints: an integrated quantitative proteomics and transcriptomics analysis of differences between slow and fast muscle fibers. *Mol. Cell. Proteomics*, **11**, M111. 010801.
90. Cox, J. and Mann, M. (2008) MaxQuant enables high peptide identification rates, individualized p.p.b.-range mass accuracies and proteome-wide protein quantification. *Nat. Biotechnol.*, **26**, 1367–1372.
91. Shevchenko, A., Tomas, H., Havlis, J., Olsen, J.V. and Mann, M. (2006) In-gel digestion for mass spectrometric characterization of proteins and proteomes. *Nat. Protoc.*, **1**, 2856–2860.
92. Wagner, S., Heseding, C., Szlachta, K., True, J.R., Prinz, H. and Hovemann, B.T. (2007) Drosophila photoreceptors express cysteine peptidase tan. *J. Comp. Neurol.*, **500**, 601–611.